Progress in Oceanography 210 (2023) 102931

Contents lists available at ScienceDirect

Progress in Oceanography

journal homepage: www.elsevier.com/locate/pocean

Cross-shelf exchange associated with a shelf-water streamer at the Mid-Atlantic Bight shelf edge

Weifeng (Gordon) Zhang [a,*], Philip Alatalo [a], Taylor Crockford [a], Andrew J. Hirzel [b], Meredith G. Meyer [c], Hilde Oliver [a], Emily Peacock [a], Christian M. Petitpas [d], Zoe Sandwith [a], Walker O. Smith Jr. [c,e], Heidi M. Sosik [a], Rachel H.R. Stanley [f], Bethany L.F. Stevens [b], Jefferson T. Turner [g], Dennis J. McGillicuddy Jr. [a]

[a] *Woods Hole Oceanographic Institution, Woods Hole, MA, USA*
[b] *Massachusetts Institute of Technology - Woods Hole Oceanographic Institution Joint Program, Woods Hole, MA, USA*
[c] *Virginia Institute of Marine Science, College of William & Mary, Gloucester Point, VA, USA*
[d] *Massachusetts Division of Marine Fisheries, New Bedford, MA, USA*
[e] *School of Oceanography, Shanghai Jiao Tong University, Shanghai, China*
[f] *Department of Chemistry, Wellesley College, Wellesley, MA, USA*
[g] *University of Massachusetts Dartmouth, Dartmouth, MA, USA*

ARTICLE INFO

Keywords:
Cross-shelf exchange
Warm-core ring
Shelf-water streamer
Heat flux
Salt flux
Carbon flux
Primary productivity

ABSTRACT

Significant exchanges between the Mid-Atlantic Bight (MAB) continental shelf and the neighboring open ocean can be induced by *shelf water streamers*, submesoscale filaments of shelf water entrained into the open ocean by Gulf Stream warm-core rings (WCRs) impinging onto the MAB continental shelf. Shelf water streamers have distinctive surface temperature and chlorophyll signals, and are thus visible from space. Satellite-measured sea surface height, temperature and chlorophyll show the evolution of a WCR over its 6-month lifespan in February-August 2019 and the persistent shelf water streamer it generated on its outskirt. *In situ* measurements from a two-week cruise in July 2019 were analyzed to investigate the physical, biological and biogeochemical characteristics of the shelf water streamer below the surface, and to quantify the associated cross-shelf transport of volume, heat, salt, carbon and oxygen. The analyses demonstrated that offshore transport of shelf water by the streamer, which was presumably balanced by either onshore intrusion of ring water or enhanced transport of shelf water from upstream, represented a major form of exchange between the MAB continental shelf and the open ocean. The streamer caused significant net onshore transport of heat and salt, and a significant net offshore transport of organic carbon and oxygen. Primary productivity in the streamer was higher than the surrounding slope and ring waters on the surface, which likely resulted from subsurface nutrients in the offshore-flowing shelf water being gradually consumed as the overlying water became clearer. WCR-induced shelf water streamers thus enhanced surface biological productivity in the slope sea.

Plain Language Summary: Waters of the shallow Mid-Atlantic Bight continental shelf and the neighboring deep slope sea have distinctly different physical, biological and chemical properties. Mixing between them can affect the shelf ecosystem and the dispersal of coastal materials into the deep ocean. One type of cross-shelf-edge mixing process results from strong clockwise-rotating vortices – so-called *warm-core rings* – formed from meanders of the Gulf Stream. As a warm-core ring intrudes onto the shelf edge, it often draws shelf water offshore, forming a thin filament in the slope sea. This filament is called a shelf-water streamer and has distinctive surface temperature and chlorophyll signals that are visible from space. Warm-core rings can also push offshore water onto the shallow shelf. This study examines the evolution of a warm-core ring over its 6-month lifespan in 2019 and the shelf-water streamer the ring induced in 5 of the 6 months. Interdisciplinary measurements from a field

Abbreviations: WCR, Warm-Core Ring; MAB, Mid-Atlantic Bight; SST, Sea Surface Temperature; SSH, Sea Surface Height; CTD, Conductivity-Temperature-Depth; PAR, Photosynthetically Active Radiation; CDOM, Colored Dissolved Organic Matter; POC, Particulate organic carbon; PON, Particulate Organic Nitrogen; TA, Total Alkalinity; ADCP, Acoustic Doppler Current Profiler; IFCB, Imaging FlowCytobot; MOCNESS, Multiple Opening/Closing Net and Environmental Sensing System; NCP, Net Community Production; EIMS, Equilibrator Inlet Mass Spectrometer; VPR, Video Plankton Recorder.

* Corresponding author at: 266 Woods Hole, WHOI MS#11, Woods Hole, MA 02543, USA.
E-mail address: wzhang@whoi.edu (W.(G. Zhang).

https://doi.org/10.1016/j.pocean.2022.102931
Received 19 August 2022; Received in revised form 25 October 2022; Accepted 22 November 2022
Available online 28 November 2022

expedition in July 2019 were examined to assess the subsurface patterns of the streamer and to quantify the induced cross-shelf fluxes of heat, salt, organic carbon and oxygen. The analysis showed that the streamer represented a major form of cross-shelf mixing and caused a substantial onshore transport of heat and salt, as well as a substantial offshore transport of organic carbon and oxygen.

1. Introduction

The Mid-Atlantic Bight (MAB) continental shelf (Fig. 1) is biologically productive (Sherman et al., 2002). The water on the shelf has Arctic and terrestrial origins (Chapman and Beardsley, 1989), and its physical and biogeochemical properties differ markedly from those in the neighboring *slope sea* (Csanady and Hamilton, 1988; Wang et al., 2013). The shelf and slope waters are separated at the shelf break by a persistent front with strong gradients in physical and biogeochemical properties (e.g., Falkowski et al., 1988; Linder and Gawarkiewicz, 1998; Vaillancourt et al., 2005; Hales et al., 2009). Exchange of water masses between the MAB shelf and open ocean can significantly affect shelf water properties (Lentz, 2010; Zhang and Gawarkiewicz, 2015), offshore dispersal of shelf materials (e.g., Walsh et al., 1988; Biscaye et al., 1994), and cross-shelf transport of marine biota (e.g., Rypina et al., 2014).

Mesoscale anticyclonic warm-core rings (WCR) shed episodically from the Gulf Stream are prominent features in the slope sea off the U.S. east coast (Saunders, 1971; Morgan and Bishop, 1977). About 25 WCRs form in the slope sea each year (Gangopadhyay et al., 2020). While only a few of them are formed in the slope sea immediately offshore of the MAB, a number of the rings formed farther to the east propagate southwestward into the MAB slope sea. When impinging on the MAB shelf edge, WCRs can induce substantial cross-shelf exchange by forcing ring water onto the shelf (Ullman et al., 2014; Zhang and Gawarkiewicz, 2015) or pulling shelf water across the shelf break into the slope sea (e.g., Joyce et al., 1992; Lee and Brink, 2010). When the latter process occurs, a pronounced cold filament of shelf water, a *shelf-water streamer* a few tens of kilometers wide, is formed and moves along the eastern periphery of the WCR (Garfield and Evans, 1987; Bisagni et al., 2019). Cherian and Brink (2016) argued that shelf-water streamers form from elevated sea surface height of WCRs propagating onto the shelf and that the associated radial sea level gradient drives a barotropic outflow on the shelf along the ring periphery. This represents an entrainment of shelf water by the ring. Through frontal subduction on the ring edges, a WCR can also drive a subsurface layer of shelf water offshore underneath the ring water, a baroclinic process undetectable at the surface (Zhang and Partida, 2018). This subsurface offshore transport of shelf water usually occurs in conjunction with shelf water streamers visible at the surface.

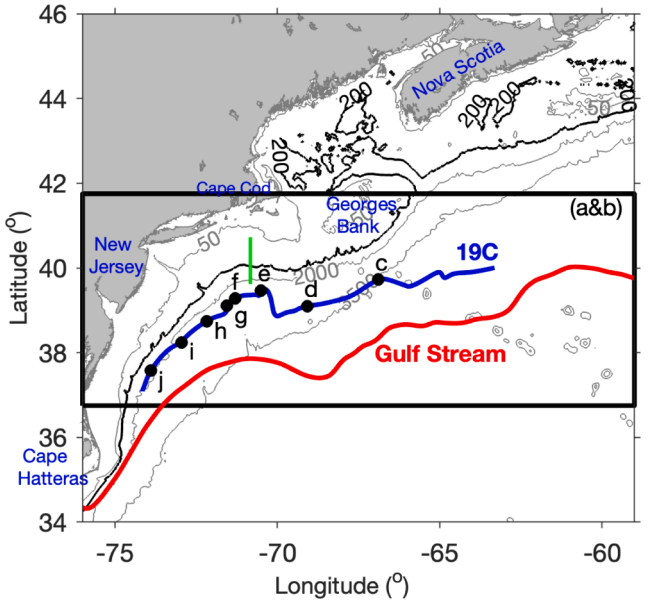

Fig. 1. The geographic region of the Mid-Atlantic Bight shelf and slope seas. The gray and black lines are isobath contours with the black line representing 200 m isobath, i.e., the shelf break; the red line the mean Gulf Stream path in February-August 2019; the blue line the track of Ring 19C over the same period; the black dots the centers of Ring 19C at the times shown in Panel c-j in Figs. 2 and 3; the green line indicates location of the CTD transect (Fig. 4); and the thick black box shows the area of view in Panel a-b in Figs. 2 and 3. (For interpretation of the references to color in this figure legend, the reader is referred to the web version of this article.)

Shelf-water streamers, together with the associated subsurface shelf-water transport, represent a pathway of MAB shelf water moving offshore into the slope sea. Joyce et al. (1992) estimated the volume transport of a shelf-water streamer induced by WCR 82B impinging onto the MAB shelf edge in June 1982 to be 0.38 Sv (1 Sv = 10^6 m^3 s^{-1}) assuming a shelf-water salinity of < 34 or 0.86 Sv assuming a shelf-water salinity of < 35. Chen et al. (2014) simulated a WCR in 2006 and estimated the ring-induced mean cross-shelf transport (including a shelf-water streamer) over a month to be 0.28 Sv. Based on satellite data in 1978–1999 and a number of assumptions about ring shape and flow, Chaudhuri et al. (2009) estimated the mean annual volume of MAB shelf water being entrained offshore by WCRs as 4000 km^3, equivalent to an annual mean shelf-water volume transport of 0.13 Sv. These values are comparable to the measured annual mean along-shelf transport over the entire MAB shelf (inside the 100-m isobath) of 0.29 Sv (Ramp et al., 1988) and the shelf-break frontal jet transport of 0.2–0.4 Sv (Linder and Gawarkiewicz, 1998).

Offshore transport of shelf water in streamers impacts the MAB shelf heat and salt budget, biogeochemistry, and ecology, but there have been few direct *in situ* measurements of streamer-associated fluxes. One exception is a study by Joyce et al. (1992) where the subsurface structure of a shelf-water streamer induced by WCR 82B was sampled. Assuming the offshore transport in the shelf-water streamer was volumetrically balanced by onshore transport of warmer and saltier slope water, Joyce et al. (1992) estimated the onshore heat and salt fluxes associated with the streamer were 1.8×10^{13} W and 0.94×10^6 kg s^{-1}, respectively. The former is greater than the maximum monthly mean ocean-to-air heat flux over the entire MAB shelf ($\sim 100 \times 800$ km^2); the latter is 1.5 times the onshore salt flux at the shelf break required to balance the MAB shelf salt budget (Lentz, 2010). *In situ* measurements also showed that the same shelf-water streamer resulted in offshore fluxes of suspended particulate matter (SPM) and dissolved oxygen (O_2) of 190 kg s^{-1} and 2.3×10^5 mol s^{-1}, respectively. Because of the higher concentrations of SPM and O_2 in shelf water, the net SPM and O_2 fluxes induced by WCR 82B were about 47 kg s^{-1}, and 2.8×10^4 mol s^{-1}, respectively, all significant compared to other major sources of those properties on the MAB shelf (Joyce et al., 1992). Due to lack of *in situ* observations, offshore transport of other biogeochemical tracers in shelf-water streamers is unknown. Shelf-water streamers could greatly impact the recruitment of commercially important fish on the MAB shelf as streamers carry substantial numbers of fish larvae from their natural habitat on the shelf to the open ocean (Flierl and Wroblewski, 1985; Myers and Drinkwater, 1989).

The Influence of WCRs on the MAB shelf is affected by the frequency of WCRs impinging on the shelf and forming shelf-water streamers. Based on a 7-year (1979–1985) satellite data set, Garfield and Evans

(1987) identified 49 WCRs in the slope sea off the MAB and Georges Bank. They estimated that shelf-water streamers were present about 70 % of the time and that about 9 % of the time there were more than one streamer present. Assuming these statistics of shelf-water streamers remain the same, the instantaneous volume, heat and material fluxes estimated for individual rings would represent quantities close to the long-term mean. In recent years, the Gulf Stream south of the MAB has become more unstable (Andres, 2016). This increase in the Gulf Stream instability has likely caused the observed increase in the number of WCRs being formed in the region (Gangopadhyay et al., 2020). As a result, it is likely that streamer transport is exerting more influence on the MAB shelf physical, biological and biogeochemical systems now than 40 years ago. Quantifying the offshore transport of shelf water, heat, salt and biogeochemical tracers in shelf-water streamers induced by more recent WCRs is critical for detecting long-term temporal variability in the exchange between the ecologically and socioeconomically important MAB continental shelf and the open ocean.

This study presents *in situ* measurements of a series of physical, biological and biogeochemical variables in a shelf-water streamer induced by a WCR formed in February 2019. The ring of interest was designated 19C, as two other rings, 19A and 19B, were present in the MAB slope sea when 19C was formed. Our *in situ* measurements provide a comprehensive depiction of the along- and cross-streamer distributions of streamer-water properties and provide an unprecedented opportunity to quantify the associated cross-shelf fluxes. Analysis of satellite data depicts the evolution of the ring over its 6-month lifespan and allows the flux estimates from the short-term observations to be extrapolated over the ring's lifespan.

2. Methods

2.1. Satellite data

Satellite-measured sea surface temperature (SST), sea surface height (SSH), and sea- surface chlorophyll (SSC) were used to provide a surface view of the evolution of Ring 19C and the associated shelf-water streamer during its occurrence (February-August 2019; Figs. 2-3). Three types of SST data were utilized: i) Microwave and Infrared (MWIR) SST daily products with a horizontal resolution of ~ 9 km (Ricciardulli and Wentz, 2004), ii) Advanced Very High - Resolution Radiometer (AVHRR) SST snapshots with a horizontal resolution of ~ 1 km, and iii) Moderate Resolution Imaging Spectroradiometer (MODIS) Aqua Level-2 SST snapshots with a horizontal resolution of ~ 1 km. The low-resolution through-cloud MWIR SST data provide an overview of the Gulf Stream and the WCRs in February-March 2019 when Ring 19C was formed (Fig. 2a-b). The high-resolution AVHRR and MODIS SST data provide a detailed view of Ring 19C and the shelf-water streamer when 19C impinged onto and moved along the MAB shelf edge from March-August 2019 (Fig. 2c-j).

Optimally-interpolated level-4 altimeter SSH data with a horizontal resolution of 0.25°×0.25° from the European Union Copernicus Marine Environmental Monitoring Service were used to show the Gulf Stream path and to track Ring 19C. The longest SSH contour of 0.5 m in the MAB slope sea was used to outline the Gulf Stream path for each day, and the daily paths were then averaged over February-August 2019 to obtain the mean Gulf Stream track (Fig. 1). WCRs were also detected as closed contours of positive SSH anomalies using the OceanEddies package

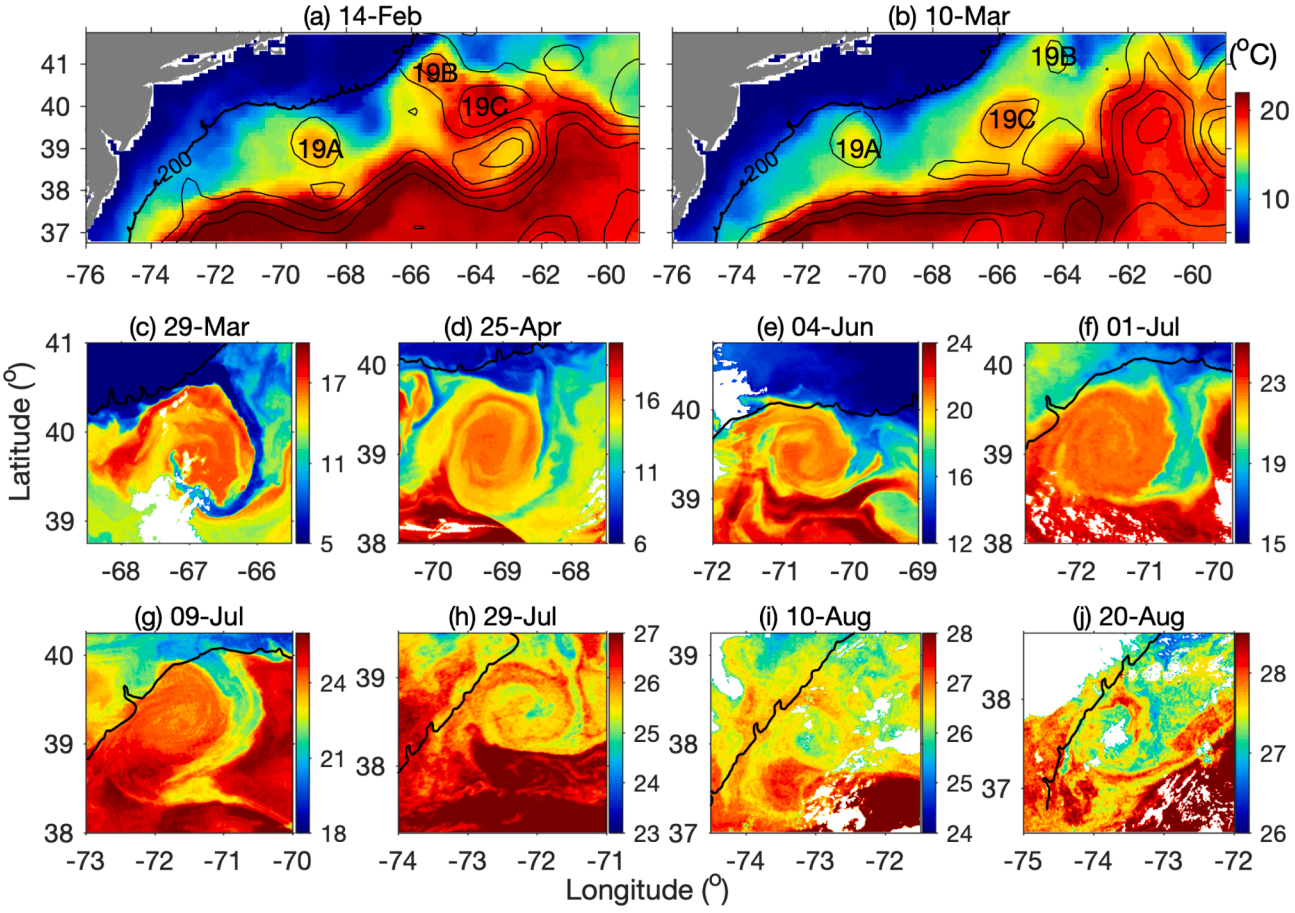

Fig. 2. Satellite-measured sea surface temperature (color) and height (thin black lines in Panels a-b) at different times over the lifespan of Ring 19C. Panels c-j are zoom-in views of the ring. The thick lines are the 200-m isobath, representing the shelf break. The labels in (a) and (b) highlight three rings in the region. Note that different color scales are used to highlight the ring.

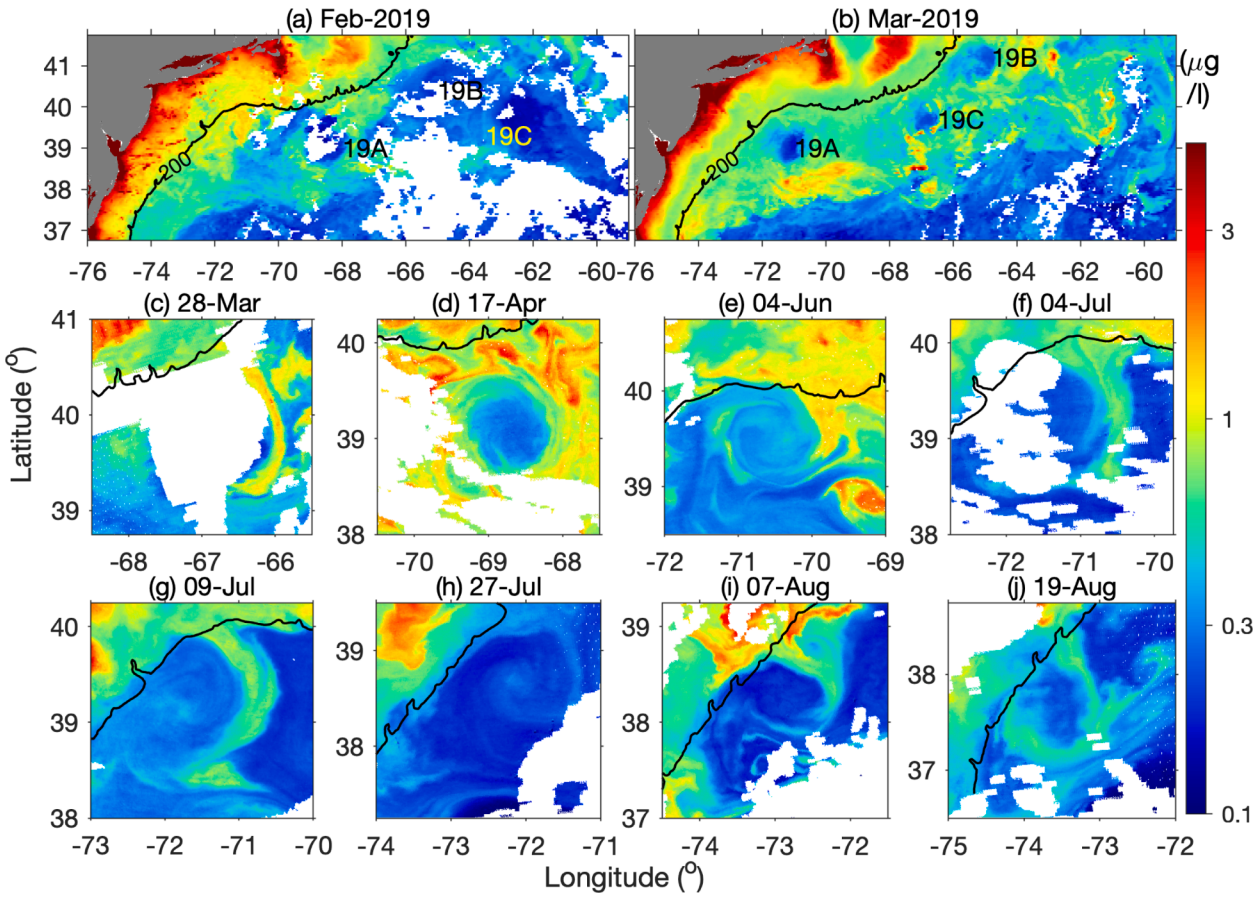

Fig. 3. Satellite-measured (a-b) monthly means and (c-j) snapshots of sea surface chlorophyll (color) at different times over the lifespan of Ring 19C. Panels c-j are zoom-in views of the ring. The black lines are 200-m isobath, representing the shelf break. The labels in (a) and (b) highlight three rings in the region.

(Faghmous et al., 2015). The daily center positions of Ring 19C were then connected to depict its track through time. The SSH data were also superimposed on the MWIR SST images to highlight the Gulf Stream and WCRs (Fig. 2a, b).

As clouds cover much of the region on any given day, monthly mean MODIS SSC data in February and March 2019 were used to show the distribution of surface chlorophyll and to highlight WCRs in the MAB slope sea (Fig. 3a-b). The daily SSC images over smaller regions were used to show the shelf water streamer of Ring 19C at different times (Fig. 3c-j).

2.2. Field observations

In situ measurements were collected during cruise TN368 of the *R/V Thomas G. Thompson* from 5 to 19 July 2019. TN368 was part of the Shelfbreak Productivity Interdisciplinary Research Operation at the Pioneer Array (SPIROPA; Smith et al., 2021; Oliver et al., 2021) project. Our original plan was to repeatedly sample a transect across the shelf break with stations ca. 7 km apart to capture the mean state and variability of the shelf break front. At the beginning of the cruise, we encountered a prominent shelf-water streamer. To examine physical and biogeochemical properties of the streamer shelf water, we adapted our plan to repeatedly sample the streamer in both cross-shelf and along-shelf (cross-streamer) directions.

A variety of continuous underway and discrete station measurements were taken to i) depict the subsurface temperature, salinity and velocity structure, and ii) quantify phytoplankton and zooplankton abundance, biological productivity, and the concentrations of biogeochemical tracers in the streamer. Phytoplankton abundance was derived from automated flow cytometry and imaging (Sosik and Olson, 2007), phytoplankton productivity from simulated *in situ* ^{14}C-uptake measurements (Smith et al., 2000), net community production (NCP) from triple oxygen and O_2/Ar methods (Stanley at al., 2015), and concentrations of biogeochemical tracers from discrete water samples collected from a Conductivity-Temperature-Depth (CTD)-Niskin rosette. Hydrographic and bio-optical properties were obtained from a towed Video Plankton Recorder (VPR; Davis et al., 2005).

We report data from two CTD transects: a north–south-oriented cross-slope transect on 06 July along 70.83°W that included 14 stations (A5-A18; Fig. 4a, c) spaced 7.2 km apart, and an east–west-oriented along-slope transect on 8 July along 39.25°N with 8 stations (S1-S8; Fig. 4b, d) spaced 10 km apart. At each station, vertical CTD profiles were taken using a CTD-rosette system equipped with 24 10-L Niskin bottles for collecting discrete water samples at 10-m intervals. The CTD SeaBird 911 system was equipped with a SBE 43 oxygen sensor, a photosynthetically active radiation (PAR) sensor (BioSpherical Instruments), a fluorometer (WetLabs FLNTURTD) and a beam transmissometer (WetLabs C-Star). Those instruments measured water column concentrations of O_2, chlorophyll, colored dissolved organic matter (CDOM) and turbidity. Concentrations of nutrients (nitrate, nitrite, phosphate, and silicic acid), chlorophyll, particulate organic carbon (POC), and particulate organic nitrogen (PON) were measured from discrete water samples. Nutrient samples were filtered through 0.4 μm polycarbonate filters, frozen in acid-washed polyethylene bottles, and analyzed post-cruise at the Woods Hole Oceanographic Institution Nutrient Analytical Facility. Chlorophyll concentrations were quantified on duplicate water samples (290 mL) that were filtered through GF/F Whatman filters under low (0.45 atm) vacuum, immediately frozen in liquid nitrogen, and thawed and extracted post-cruise in 90 % acetone and analyzed by standard fluorometric methods (JGOFS, 1996). POC

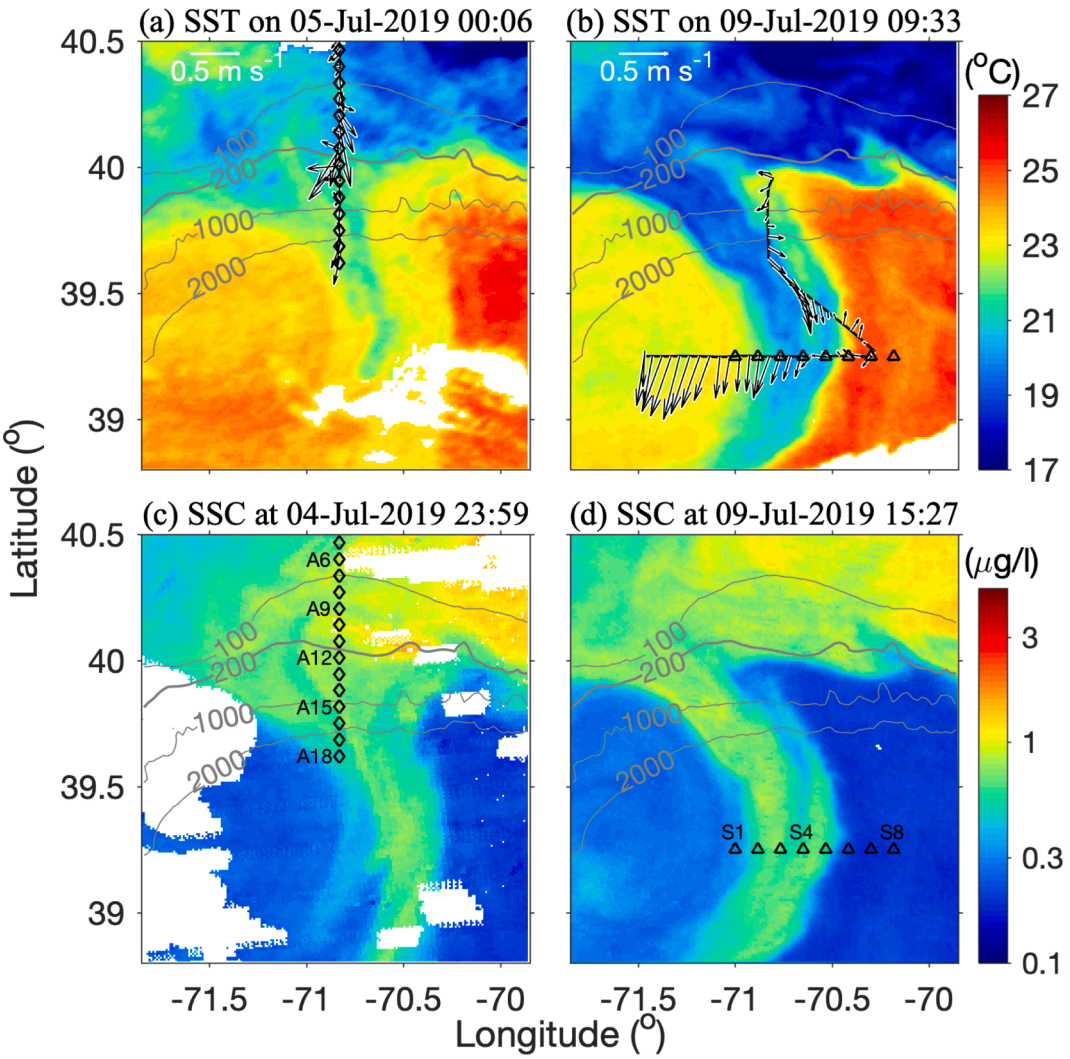

Fig. 4. Zoom-in views of the satellite-measured sea surface temperature (top) and chlorophyll (bottom) around the times of the *in situ* measurements. The diamonds in the left panels show locations of Stations A5-A18; the triangles in the right panels show locations of Stations S1-S8; the black lines in (b) show the track of the VPR tow on July 7; the arrows in (a) and (b) show horizontal velocity at 36 m measured by the ship-board ADCP; The white arrows in (a) and (b) are scales of the velocity vectors; the gray lines are 100, 200, 1000, and 2000 m isobaths.

and PON concentrations were assessed by filtering 0.25–2.0 L of seawater under low vacuum through precombusted (450 °C for 2 h) Whatman GF/F filters (Gardner et al., 2000), stored in precombusted glass vials, dried at 60 °C, and analyzed on a Costech ECS Model 4010 elemental analyzer. All profile data were interpolated onto a horizontal grid of 2 km and vertical grid of 1 m for visualization and flux calculations.

Discrete samples for total dissolved inorganic carbon (TCO_2) and total alkalinity (TA) were collected at selected stations following recommended best practices (Dickson et al., 2007) in borosilicate glass bottles and immediately fixed with a solution of supersaturated mercuric chloride ($HgCl_2$). TCO_2 was analyzed by nondispersive infrared detection using an Automated Infrared Inorganic Carbon Analyzer (Marianda); TA was analyzed using an open-cell potentiometric titration (with components from Metrohm). Analysis of certified reference materials from A. G. Dickson (Scripps Institution of Oceanography) ensured that the uncertainty (accuracy and precision) of the TCO_2 and TA measurements was better than 2 and 3 μmol kg^{-1}, respectively. Following measurement of TCO_2 and TA, pH and pCO_2 were computed using the CO_2sys program of van Heuven et al. (2011), and phosphate and silicate concentrations were used in the carbonate system computations as recommended.

Hydrographic and bio-optical data were collected using a towed VPR equipped with a CTD (SBE 49 FastCat), oxygen sensor (SBE 43), fluorometer (ECO FLNTU-4050), ECO Triplet (ECO BBFL2-123), and a PAR sensor (Biospherical Instruments Inc. QCP-200L). The VPR was towed in a coat-hanger pattern (hereafter referred to as the *coat-hanger transect*; solid line Fig. 4b) on 7 July. The southernmost leg of the coat-hanger transect was oriented east–west and transected the streamer. The VPR undulated between 5 and 100 m as the ship moved at ca. 10*kt* ($1kt \approx 0.51 ms^{-1}$). The mean horizontal distance between neighboring up- and down-casts was ~ 450 m; for visualization and flux calculations, the profiles were interpolated onto a vertical grid with 1-m resolution.

Velocity data from a ship-mounted OS75 Acoustic Doppler Current Profiler (ADCP) were used to quantify the along-streamer transport. The ADCP was configured with the University of Hawai'i Data Acquisition System (UHDAS) with 8-m vertical bins and 15-minute averaging windows, and the underway velocity data were processed with the Common Ocean Data Acquisition System (CODAS). The barotropic tidal flow at M2, S2, N2, K2, K1, O1, Q1 and M4 frequencies extracted from the Oregon State University Tidal Prediction Software (OTPS; Egbert and Erofeeva, 2002) were removed from the velocity data. The ADCP configuration gives a near-surface vertical blanking range of 35m with no velocity data. To calculate the cross-transect transport of the shelf

water over the entire depth range, we combined the measured density distribution with a thermal-wind balance to compute the cross-transect component of the velocity in the blanking range.

Phytoplankton were observed with a combination of flow cytometry and imaging-in-flow cytometry (Sosik et al. 2010). Instruments were configured to automatically sample the near-surface water at regular intervals from the ship's flowing seawater system. Pico- and nanoplankton were measured with an Attune NxT Flow Cytometer (ThermoFisher Scientific) configured with two lasers (488 nm, 532 nm), fluorescence channels for chlorophyll (680 nm) and phycoerythrin (575 nm), and two side angle light scattering sensitivities (OD2 neutral density filter added for high sensitivity at 532 nm). The Attune was adapted to sample 0.4 mL automatically every 2 min. Nano-and microplankton were measured with Imaging FlowCytobot (IFCB; McLane Research Laboratories, Inc.). Individual cell light scattering signals were converted to cell volume with calibration from cell cultures independently sized on a Coulter Multisizer. The IFCB was configured to automatically sample 5 mL at ~ 25 min intervals. Images were automatically analyzed and assigned to taxonomic groups following approaches developed for the IFCB time series at the Martha's Vineyard Coastal Observatory (Sosik et al., 2016). The measured phytoplankton were separated into three size classes according to equivalent spherical diameter computed from biovolumes: <2 μm (pico), 2–20 μm (nano), and > 20 μm. Cell biovolume was also estimated from the Attune and IFCB images (Moberg and Sosik 2012) and converted to cell carbon following the relationships described by Menden-Deuer and Lessard (2020). Combining the cell carbon with chlorophyll concentrations measured from all surface water bottle samples of the cruise gives a phytoplankton carbon-to-chlorophyll ratio of 166 (Fig. 5), which will be used to calculate cross-shelf algal carbon fluxes induced by the streamer (Section 4.3).

Zooplankton were sampled at selected stations using a Multiple Opening/Closing Net and Environmental Sensing System (MOCNESS) with a 0.5 m^2 mouth area (Wiebe et al., 1976). The first net sampled from the surface down to the maximum sampling depth at that station, and the other nets sampled at discrete depths. At each station, 3 epipelagic depths (shallower than 100 m) were sampled based on the CTD fluorescence profiles: the surface, the subsurface chlorophyll maximum, and below the subsurface chlorophyll maximum. All three depths were sampled with 150 μm-mesh nets for 2 min and an additional sample was collected at the subsurface chlorophyll maximum using a 100 μm-mesh net. A calibration was conducted at the end of the cruise consisting of two separate half-kilometer tows in opposite directions at 30-m depth, to confirm flow-meter readings with distance traveled. This allowed calculation of the volume of water sampled during each MOCNESS tow. After retrieval, nets were washed down with a saltwater deck hose to concentrate zooplankton into net cod ends. Samples were then transferred to one-liter jars and preserved in approximately 10 % formalin:seawater solutions for microscopic analyses ashore. At the shore-based laboratory, samples were drained through 64 μm-mesh sieves for removal of formalin:seawater and the concentrated zooplankton were transferred to 70 % ethanol for microscopic identification and enumeration as described in Petitpas et al. (2014).

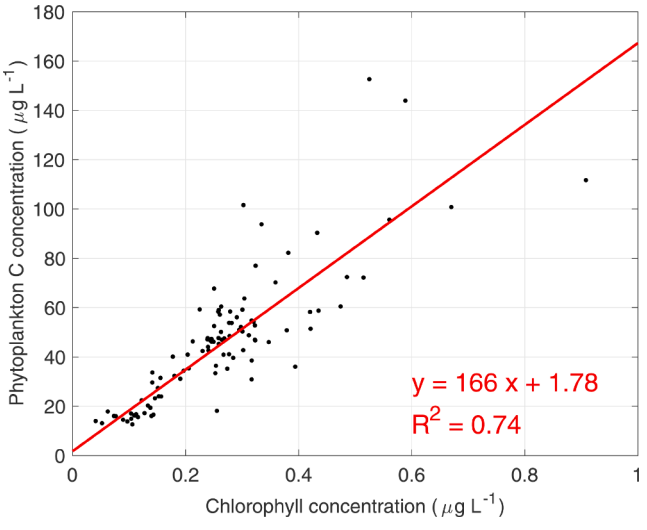

Fig. 5. Attune and IFCB-based phytoplankton carbon concentration vs chlorophyll concentration measured from the surface water bottle samples during cruise TN368. The red line represents a least-squares fit to all the data. (For interpretation of the references to color in this figure legend, the reader is referred to the web version of this article.)

2.3. Measurements of biological productivity

To compare biological productivity of the streamer shelf water and the surrounding slope and ring waters, rates of photosynthetic carbon assimilation and net community production (NCP) were measured. Primary productivity was also estimated using a bio-optical model (Ma and Smith, 2022). These methods together provide a holistic description of the biological productivity within and outside of the streamer. Details of the methods are described in Smith et al. (2021), Oliver et al. (2021), and Ma and Smith (2022). Simulated *in situ* incubators and ^{14}C-uptake measurements were used to obtain the rate of photosynthetic carbon assimilation at discrete depths at selected stations. Approximately 20 μCi $NaH^{14}CO_3$ (pH = 9.6) was added to water samples taken from different isolumes and placed in sterile 280-mL Qorpak bottles. The bottles were then placed in irradiance-simulating Plexiglas tubes wrapped with blue and neutral density screening. The tubes were submerged in a deck incubator with a surface seawater flowing system to maintain surface temperatures. After 24 h, water samples were filtered through GF/F filters, which were then placed in scintillation vials, to which 5 mL Ecolume® scintillation cocktail was added, placed in darkness for 24 h, and counted on a Beckman liquid scintillation counter.

Vertical profiles of productivity were also estimated using a bio-optical model based on the formulation of Behrenfeld and Falkowski (1997a, b). The calculation combines measured profiles of temperature, fluorescence, and PAR, along with a global temperature-photosynthesis response and the euphotic depth (Oliver et al., 2021). At the incubation stations on both the along- and cross-slope transects, vertical profiles of primary productivity given by the bio-optical model match the pattern of the incubation-based productivity measurements (Fig. 6). The model-estimated high-resolution productivity profiles show vertical variability with length scales similar to that of chlorophyll.

To calculate high spatial resolution (~2 km) NCP in surface waters, dissolved oxygen and argon concentrations were measured by an Equilibrator Inlet Mass Spectrometer (EIMS) from the ship's flowing seawater system with a precision of 0.2 % on a timescale of seconds to minutes. The EIMS system was designed following Cassar et al. (2009) with modifications described in Smith et al. (2021). Rates of NCP were calculated from the continuous O_2/Ar data as

$$NCP = \left[(O_2/Ar)_m/(O_2/Ar)_e - 1\right] \times O_{2e} \times k \times \rho$$

where $(O_2/Ar)_m$ is the O_2 to Ar ratio measured by the EIMS, $(O_2/Ar)_e$ the ratio of O_2 to Ar equilibrium concentrations, k the gas transfer velocity, ρ the density of seawater, and O_{2e} the equilibrium concentration of O_2 (Stanley et al., 2015). The NCP calculation assumes a steady state and represents a mixed-layer *integrated* rate of biological production with a spatial resolution of a few kilometers over the time scale of a few days. The calculations do not include effects of vertical mixing since we do not have O_2/Ar depth profiles at the same spatial resolution as the EIMS data. However, at the CTD stations where O_2/Ar profiles were measured, vertical mixing corrections were calculated using the method

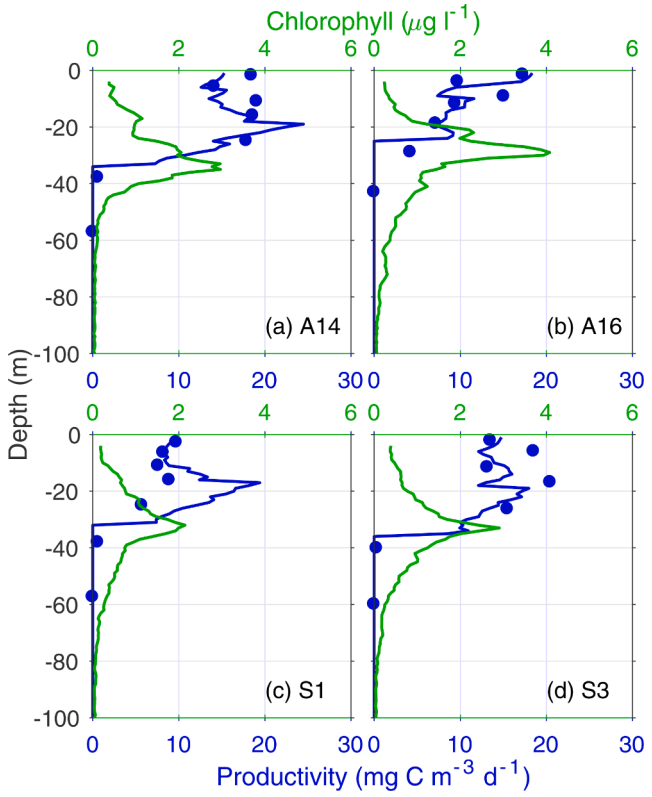

Fig. 6. Vertical profiles of chlorophyll concentration (green lines), ^{14}C-uptake primary productivity (blue dots), and primary productivity estimated by the bio-optical model (blue lines) on the (a-b) cross-slope and (c-d) along-slope transects. (For interpretation of the references to color in this figure legend, the reader is referred to the web version of this article.)

described in Seguro et al. (2019) and found to be<10 % of the NCP rates. In order to not bias the data by including corrections at some locations and not others, vertical corrections were not included in any of the NCP calculations.

3. Observed patterns

3.1. Surface patterns of temperature and chlorophyll

Ring 19C first separated from the Gulf Stream in February 2019 in the slope region to the southeast of Georges Bank, around 64°W, 40°N (Figs. 1 and 2). It then migrated westward. At the end of March, it moved northward and came into contact with the southern flank of Georges Bank (Figs. 1 and 2c). Thereafter, it migrated westward/southwestward along the MAB shelf break in a trajectory similar to Ring 82B (Fig. 1 in Evans et al., 1985). By the end of August, it reached the narrow slope region between the southern end of the MAB shelf edge and the Gulf Stream; the ring center was at 74°W, 37.5°N. Six months after its formation, it was reabsorbed into the Gulf Stream. As Ring 19C migrated along the shelf edge toward the southwest, its surface temperature increased gradually, presumably due to seasonal heating, while the signal of its elevated surface temperature relative to the surrounding water became less distinct (Fig. 2). The surface chlorophyll concentrations in the central region of the ring remained relatively low (<0.3 μg/L) throughout the 6-month period (Fig. 3).

After impinging onto the southern flank of Georges Bank at the end of March, Ring 19C induced a prominent streamer, as indicated by a narrow band of cold shelf water with a relatively high concentration of chlorophyll on its eastern flank (Fig. 3). The streamer stretched from its *root* (the shelf end of the streamer at 200-m isobath) along the eastern/northeastern edge of the ring into the slope sea and persisted for about 5 months until it merged into the Gulf Stream at the end of August. In August, as Ring 19C migrated toward the warm slope water in the southern MAB, the temperature signal of the shelf-water streamer became less pronounced (Fig. 2i-j), while its chlorophyll signal remained distinct (Fig. 3i-j). At times, the streamer appeared to wind toward the ring center forming an inward spiral pattern (e.g., Figs. 2d, h, 3e, h), but this pattern was not persistent. In general, the surface temperature gradually increased and the surface chlorophyll slowly decreased relative to the shelf source.

The gradual along-streamer increase of surface temperature and decrease of surface chlorophyll are evident during the TN368 cruise in July 2019 (Fig. 4). On 05 July, the surface temperature at the shelf end of the streamer at 40°N (~200-m isobath) was about 20 °C. It gradually increased southward along the streamer reaching 24 °C at 39°N. On 09 July, the surface temperature at the streamer root was 19 °C, and it gradually increased to 21 °C at 39°N. There was a decrease in SST over the entire region from 05 to 09 July, which resulted from region-wide heat loss to the atmosphere during a period with low air temperatures, low solar radiation, and relatively strong winds on 08 July (Fig. 7). On 04 July, the surface chlorophyll at the root of the streamer was about 1 μg L^{-1}, and it decreased gradually southward along the streamer to 0.5 μg L^{-1} at 39°N (Fig. 4c). These changes of the surface properties in the streamer could represent dilution of the streamer shelf water through mixing with the surrounding slope or ring water, which would affect biological productivity in the streamer (see Section 4.2).

3.2. Cross-shelf distribution

Data from the cross-shelf CTD transect (Fig. 4a) on 06 July captured the subsurface transition of physical and biogeochemical properties from the shelf water to the offshore-moving streamer water (Figs. 8, 9). At this time, the root of the streamer was at the 200-m isobath and ~40°N, close to Station A12. On the shelf end (onshore of the 100-m isobath; Stations A5-A7), the entire water column consisted of shelf water with salinity<33 (Figs. 8b, 10b). The shelf water temperature was low, except in a thin surface layer (Figs. 8a, 10a). Between the 100- and 200-m isobaths (Station A5-A12), the base of the shelf water lifted off the bottom; isopycnals (Fig. 8c) and the 34.5 isohaline, an indicator of the base of the shelf water (Figs. 8, 9), rose from A8 to A12. Farther offshore, isopycnals and the 34.5 isohaline were relatively flat. At the offshore end of the transect (Station A18), shelf water occupied the upper 50 m of the water column. Shoaling of the isopycnals and the 34.5 isohaline between the 100- and 200-m isobaths was consistent with the structure of the baroclinic shelf break front in the region (e.g., Linder and Gawarkiewicz, 1998). Meanwhile, subsurface salinity in the streamer increased gradually offshore, which could result from gradual dilution of the shelf water by the surrounding ring and slope waters of higher salinity, or from the cross-streamer variation. Note that the cross-shelf transect did not completely align with the along-streamer direction, and some of the cross-shelf variability, such as the isolated subsurface patch of high temperature and high salinity at 39.95°N, resulted from cross-streamer (along-shelf) variation. Regardless, the majority of the cross-shelf variability should reflect along-streamer variations in water properties, which are much greater than those of the ambient water in the cross-streamer direction (see Section 3.3).

A westward jet with a core speed of 0.4 m s^{-1} was located around 40°N between Stations A11 and A13 (Fig. 8g). There was also an eastward flow at 40.2°N, which together with the westward frontal jet, formed a frontal eddy at the shelf end of the streamer (Figs. 4a and 8g).

Subsurface chlorophyll and O_2 maxima occurred at 10–40 m over the entire transect (Figs. 8d-e, 10c-d). The subsurface maximum concentrations of chlorophyll and O_2 on the shelf side reached 5 μg L^{-1} and 335 *μM*, respectively, both higher than those on the offshore end. This was consistent with the elevated productivity in the subsurface layer on the shelf side (Fig. 9c). The peak subsurface production rate at Station A6 on

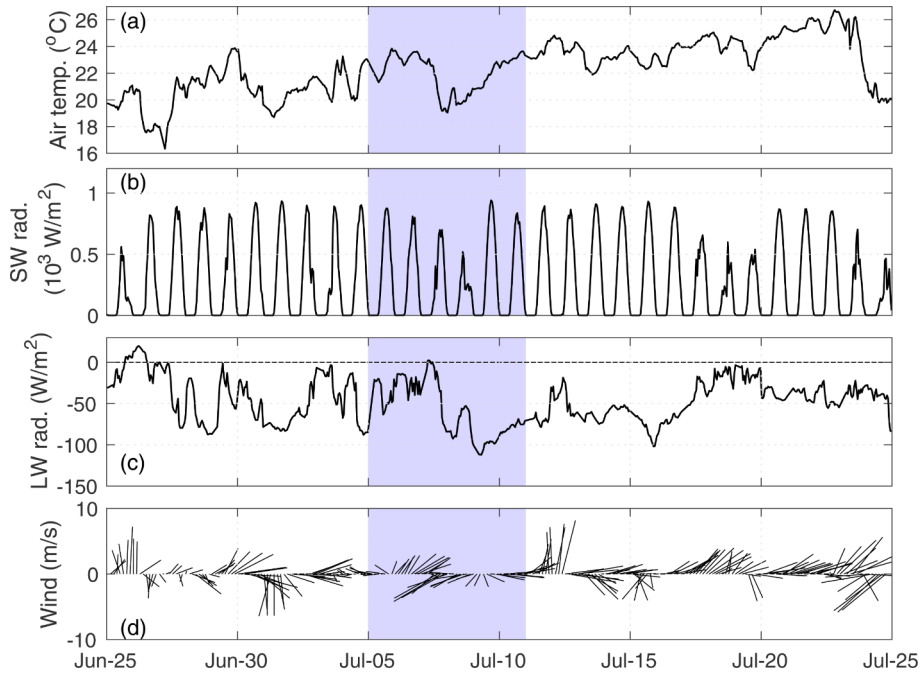

Fig. 7. Measured (a) air temperature, (b) shortwave radiation, (c) longwave radiation, and (d) wind conditions during June-July 2019. The purple area highlights the period that *in situ* measurements of the shelf water streamer of Ring 19C were collected. (For interpretation of the references to color in this figure legend, the reader is referred to the web version of this article.)

the shelf end reached 60 $mg\,C\,m^{-3}\,d^{-1}$, >4 times greater than that at Station A18 on the offshore end (Figs. 9c, 10h).

CDOM fluorescence was high throughout the water column on the shelf and decreased gradually offshore (Fig. 8f). Its distribution outlined the shelf water volume on the transect and reflected either the gradual dilution of the streamer shelf water toward offshore or cross-streamer variation in the CDOM distribution. The subsurface chlorophyll maximum overlapped with that of the nutricline, which was characterized by strong vertical gradients in nitrate (NO_3), phosphate (PO_4), and silicate (SiO_4) (Fig. 9a,b,d). Within the upper 20 m over the entire transect, NO_3 concentrations were ~ 0.05 μM, while PO_4 concentrations were ~ 0.1 μM (Fig. 10e-f). Below the surface layer, there was abundant NO_3 and PO_4 across the entire transect. The SiO_4 concentration was 1–2 μM in the upper 20 m; subsurface SiO_4 concentrations on the shelf were very high, reaching 11 μM below 40 m (Fig. 9d, 10g).

The distributions of PON and POC were similar to those of chlorophyll with a subsurface maximum at 20–40 m across the transect, and maximum concentrations of 5 and 30 $\mu mol\,L^{-1}$ at the shelf break (Fig. 9e-f). The distribution of DIC showed a similar vertical gradient across the entire transect (Fig. 9g). In the upper 20 m, the DIC concentration was ~ 2.05 $mmol\,L^{-1}$. The pH exhibited subsurface maxima at 20–40 m with peak values reaching 8.13 on the offshore end of the transect (Fig. 9h).

Cross-shelf metazoan zooplankton communities varied both with depth and also along the streamer. MOCNESS samples at Station A12 (near the 200 m isobath) on 07 July had total zooplankton abundances of ~ 10,000, ~22,000, and ~ 1,000 animals m^{-3} at the surface, 21 m and 32 m, respectively (Fig. 11a). Note that the subsurface chlorophyll maximum at A12 was at 20–30 m (Fig. 10c). Zooplankton abundance below the chlorophyll maximum was at least an order of magnitude lower than in the water column above. The community composition at all three depths was characterized by taxa typical of shelf water in the northwestern Atlantic, such as copepods of the genera *Calanus, Pseudocalanus, Paracalanus, Centropages,* and *Oithona,* as well as meroplankton (i.e., bivalve, decapod and gastropod larvae). *Oithona similis*, particularly copepodite stages, overwhelmingly dominated the zooplankton abundance. Further offshore at Station A14 (just inshore of the 1000 m isobath), MOCNESS samples (100 μm-mesh) on 06 July had a zooplankton abundance of 133 animals m^{-3} at 38 m, which was within the subsurface chlorophyll maximum, and represented the shelf water environment. At 57 m (150 μm-mesh), which was below the 34.5 isohaline representing the slope water environment, the total zooplankton abundance was 209 animals m^{-3} (Fig. 11b). Therefore, the abundance at the offshore station, A14, was at least 1–2 orders of magnitude lower than at the inshore station, A12. At A14, the shelf-water layer at the surface was overwhelmingly dominated by *Oithona similis* (81 %), with *Oithona atlantica*, a more oceanic species, comprising only < 1 % of total abundance. In contrast, *Oithona atlantica* comprised a substantial proportion (>18 %) of the zooplankton community in the deeper slope-water layer. Meanwhile, meroplankton were present at ~ 2 % of the total zooplankton abundance within the shelf-water layer, while they were completely absent in the deeper slope water layer, demonstrating offshore transport of invertebrate larvae of potential commercial importance away from coastal nursery habitats.

3.3. Cross-streamer distributions

The along-slope CTD transect on 8 July sampled a cross-section of the shelf water streamer at a location to the eastern end of WCR 19C and ~ 83 km south of the root of the streamer at the 200-m isobath (Fig. 4d). At this location, the streamer was 50 km wide and 50 m thick, as determined by the 34.5 isohaline (Figs. 12, 13). The western 15-km section of the streamer on its inner side (from the perspective of the ring center) was a thin layer of shelf water occupying the surface 5–15 m. This thin surface layer of shelf water likely resulted from westward surface Ekman transport induced by the southwestward wind on 07 July (Fig. 7). Immediately below the thin surface layer of shelf water was high-temperature and high-salinity ring water (Figs. 12a-b, 14a-b). This vertical distribution of the shelf and ring water indicates that density of the shelf water at this time was either slightly lower than or similar to that of the surface ring water (Fig. 12c). This is consistent with the observed offshore transport of shelf water at this time being entirely in a surface layer, i.e., no subduction of shelf water underneath ring water (see Section 4.1). At the core of the shelf water streamer, salinity was 33

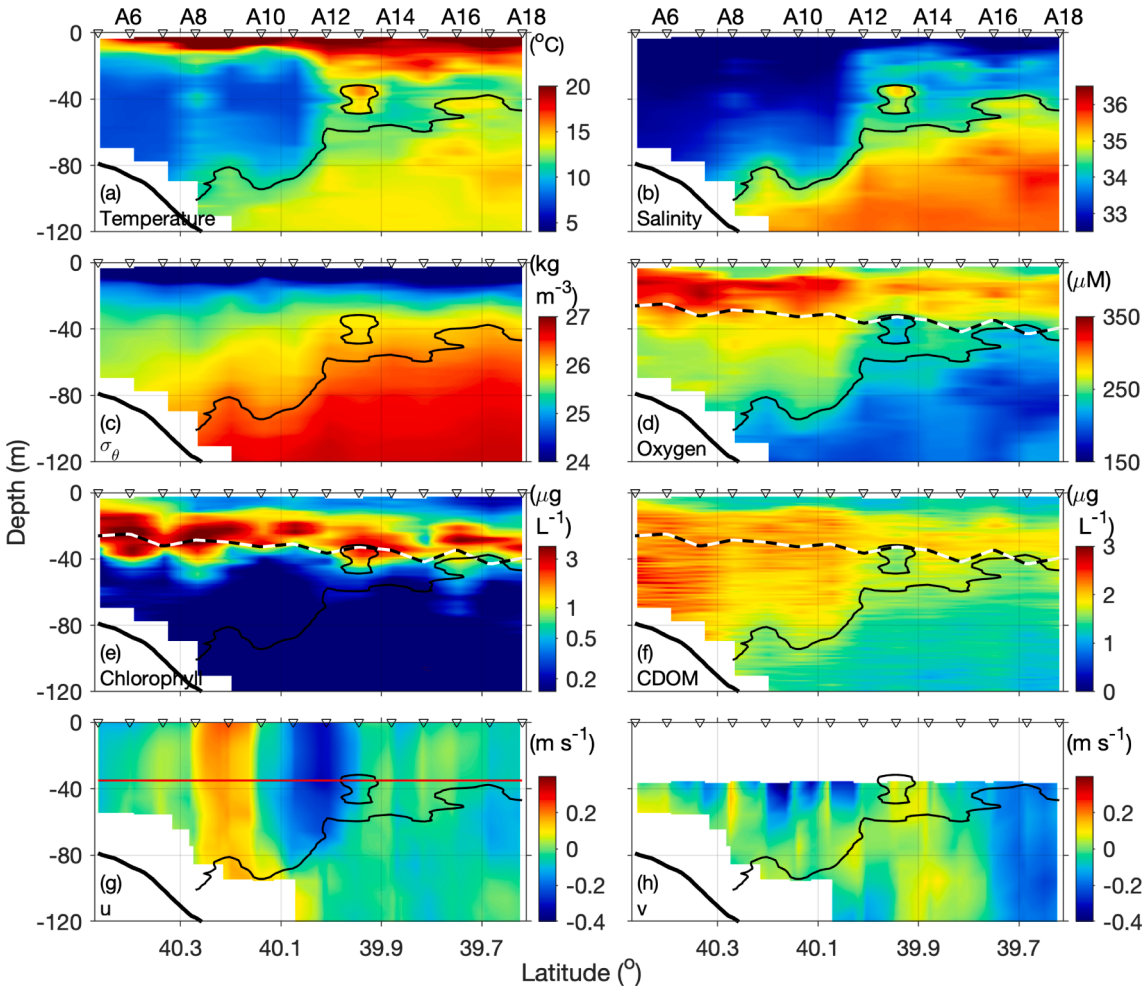

Fig. 8. Vertical distributions of (a) temperature, (b) salinity, (c) σ_θ, (d) oxygen, (e) chlorophyll, (f) colored dissolved organic matter (CDOM), (g) eastward velocity, and (h) northward velocity along the cross-shelf transect on 06 July 2019. The thin black lines are the 34.5 isohaline representing the boundary between the shelf and offshore waters. The triangles at the top of each panel represent CTD station locations. The thick black lines represent the seafloor. The black-white dashed lines represent the base of the euphotic layer; the red line in (g) separates the ADCP-measured *u* and that computed from thermal-wind balance. (For interpretation of the references to color in this figure legend, the reader is referred to the web version of this article.)

in the top 15 m, and the subsurface isopycnals were elevated compared to the slope water to the east (Fig. 12c). The velocity in the streamer was mostly southward, along with the mesoscale anticyclonic (clockwise) flow of the ring (Figs. 4b, 12h). The southward flow gradually weakened on the eastern side of the streamer and disappeared on its eastern (outer) edge. The eastern edge of the streamer thus represented the outer boundary of the ring influence. Integrating velocity from the ship-board ADCP in the cross-sectional area determined by the 34.5 isohaline gave an offshore volume transport of shelf water in the streamer of ~ 0.26 Sv.

Across the streamer, there were distinct subsurface chlorophyll and O_2 maxima at 15–30 m, shallower than those in the ring and slope waters on the western and eastern sides (Figs. 12d-e; 14c-d). The maximum O_2 concentration in the streamer reached 290 *mM*, much greater than those in the slope and ring waters (Figs. 12d, 14d). The subsurface chlorophyll maximum on the eastern side of the streamer resided at 40–55 m, below the surface slope water, while that on the western side of the streamer was at 30–40 m, below the intermediate layer of ring water, which was below the thin surface layer of streamer shelf water. The chlorophyll maximum in the streamer was 2.3 $\mu g\,L^{-1}$, similar to the maximum concentration in the ring water, but lower than that in the slope waters of 12 $\mu g\,L^{-1}$ (Figs. 12e, 14c). This elevated chlorophyll concentration in the slope water on the eastern side of the streamer (Station A7) occurred in a thin layer and resulted from upwelling of nutrient-rich subsurface Gulf Stream water that stimulated biological production (Oliver et al., 2021). The maximum productivity at Station A7 was ~ 150 $mg\,C\,m^{-3}\,d^{-1}$ at 45 m (Figs. 13c, 14h); in contrast, the subsurface productivity maximum in the streamer shelf water was 30–40 $mg\,C\,m^{-3}\,d^{-1}$ at 20 m at Stations S4 and S5. The subsurface productivity at Station S1 reached 20 $mg\,C\,m^{-3}\,day^{-1}$ at 20 m, and is below the thin surface layer of shelf water and thus in the ring water (Figs. 13c, 14h). Meanwhile, the subsurface CDOM fluorescence in the streamer shelf water remained higher than that in the neighboring ring and slope waters (Fig. 12f).

Over the entire cross-streamer section, the subsurface chlorophyll and O_2 maxima mostly overlapped with the nutricline, which was also vertically elevated in the streamer relative to the neighboring ring and slope waters on either side (Fig. 13). The NO_3 concentration in the surface layer was 0.04 μM across the transect, and the NO_3-depleted surface layer was only 15 m thick in the streamer, and 30 m thick in the slope and ring waters. PO_4 concentrations in the surface layer change across the transect from 0.08 μM in the surface streamer shelf water to 0.015 μM in the surface slope and ring waters (Fig. 14f). PO_4 was not depleted in the surface streamer shelf water, but was depleted in the surface slope and ring waters. SiO_4 concentration was ~ 1 μM in the surface streamer and ~ 0.75 μM in the surface ring and slope water.

Both PON and POC exhibited subsurface maxima at 10–30 m in the streamer, shallower than in the ring and slope waters (Fig. 13e-f). The peak PON and POC concentrations in the streamer were 3 and 18

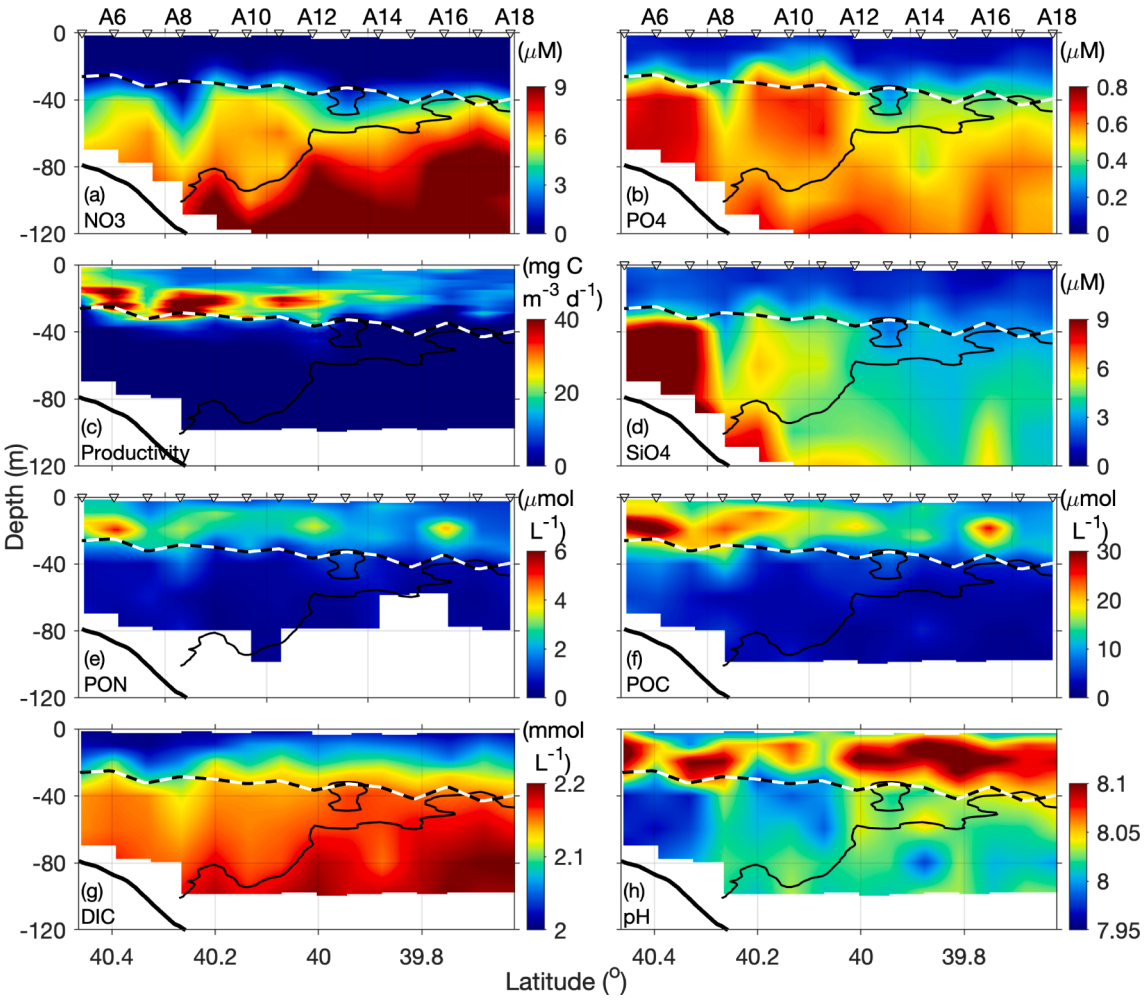

Fig. 9. Vertical distributions of (a) nitrate (NO_3), (b) phosphate (PO_4), (c) modeled primary productivity, (d) silicate (SiO_4), (e) particulate organic nitrogen (PON), (f) particulate organic carbon (POC), (g) dissolved inorganic carbon, and (h) pH along the cross-shelf transect on 06 July 2019. The thin black lines are the 34.5 isohalines representing the boundary between the shelf and offshore waters. The triangles on the top of each panel represent CTD station locations. The black-white dashed lines represent the base of the euphotic layer; the thick black lines represent the seafloor.

μmol L^{-1}, respectively, both of which were higher than the peak values in the slope and ring waters. There was a clear vertical gradient in DIC concentration, being 2.05 mM in the surface 15 m in the streamer and 2.1 mM in the surface 25 m in the slope water to the east (Fig. 13g). pH was generally higher in the streamer shelf water than in the neighboring slope water, with peak pH values in the streamer reaching 8.13 at 25 m at Stations S4 and S5, while in the slope water the maximum was 8.08 at 40 m at Station S7.

On 08 July MOCNESS samples were taken at Station S1 (Fig. 4d) where a thin layer (<10 m) of streamer water sat over the ring water. At all sampled depths (surface, 25 m and 38 m), zooplankton community composition was diverse with species of shelf, offshore, and tropical origins, but the total zooplankton abundance was < 30 animals m^{-3} (Fig. 11c), much lower than at Stations A12 and A14. Consistent with Station A14 (Fig. 11b), *Oithona similis* dominated the streamer shelf water community at the surface, comprising ~ 67 % of total zooplankton abundance. In the ring water below, the zooplankton community included a variety of offshore or tropical species, such as, copepods of the genera *Corycaeus*, *Euchaeta,* and *Sappharina*; the copepod species *Temora stylifera* and *Acartia danae*; and non-copepod taxa such as the sergestid shrimp *Lucifer faxoni*, eel leptocephalus larvae, and the chaetognath *Sagitta enflata*. Meanwhile, *Oithona similis* comprised only 26 % and 5 % of the zooplankton abundance, respectively. This subsurface composition in the ring water differed drastically from that in the subsurface slope water layer at Station A14.

3.4. Three-dimensional pattern

The VPR coat-hanger transect consisted of both along- and cross-streamer sections, and provided a 3-dimensional view of the shelf water streamer (Fig. 15). The general pattern depicted by the VPR data was consistent with that obtained from the CTD transects. At 100-m water depth (40.2°N), the streamer shelf water occupied the upper 70 m of the water column, and the streamer shelf water layer gradually shoaled toward the south and reached 50 m thick at the cross-streamer section of the transect (39.25°N). The western end of the southern leg of the VPR tow (westward) reached 71.5°W, farther into the interior of Ring 19C than the cross-streamer CTD transect. A stronger southward current was observed as the ship moved toward the ring interior (Fig. 4b, 15h). The hydrographic measurements showed vertical structures of temperature, salinity and density of the interior ring water similar to those of the water on the eastern edge of the ring, except the thermocline and pycnocline toward the ring interior were slightly deeper (Fig. 15a, c). This confirmed that the shelf water density was similar to the surface ring water. Toward the ring interior, the subsurface chlorophyll, turbidity and O_2 maxima persisted but deepened slightly.

The VPR data showed fine-scale variability in both along- and cross-streamer directions. Tilted filaments of warm (cold) and saline (fresh)

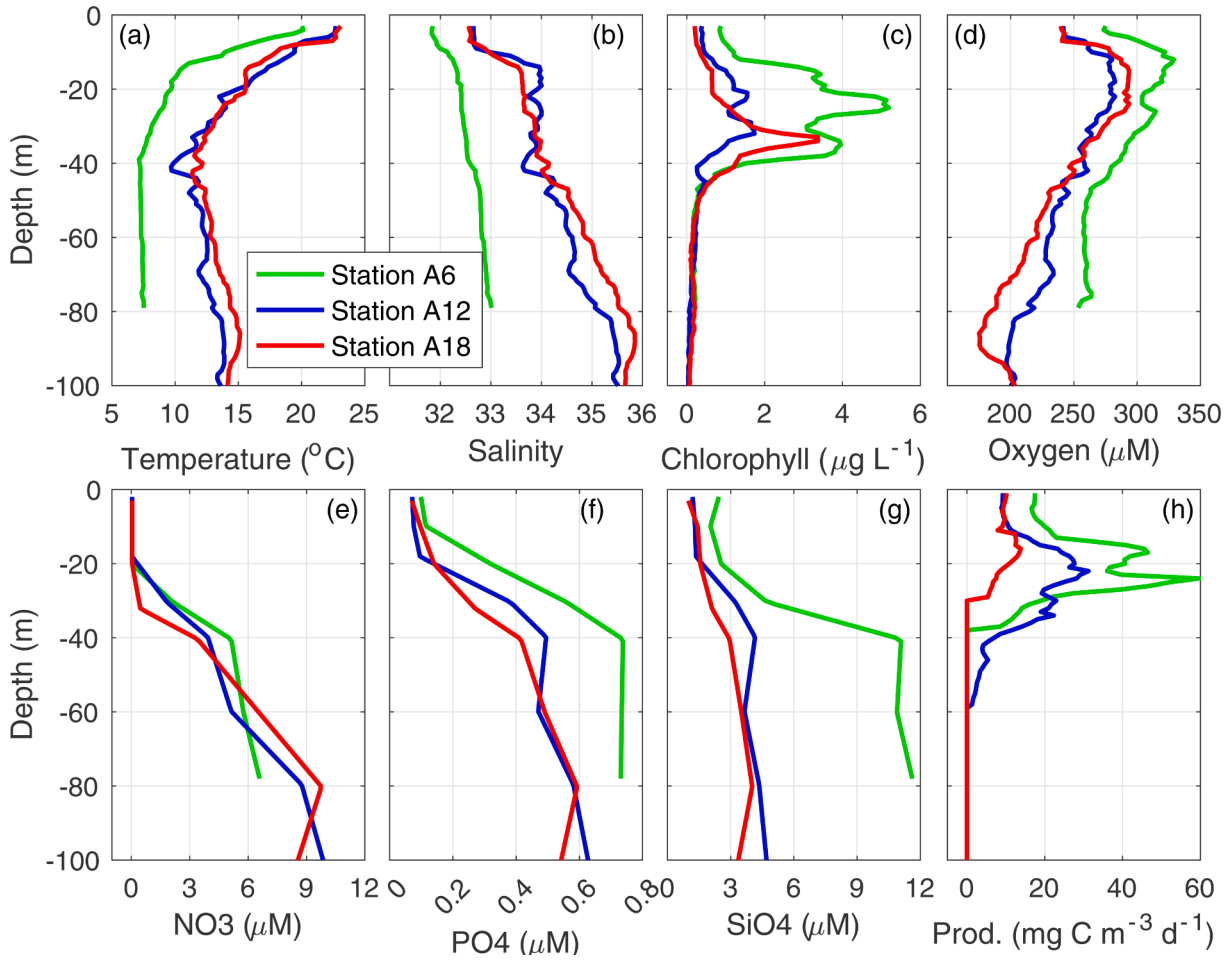

Fig. 10. Vertical profiles of (a) temperature, (b) salinity, and (c) chlorophyll, (d) dissolved oxygen, (e) nitrate, (f) phosphate and (g) silicate concentration, and (h) model-estimated productivity at Stations A6, A12 and A18, representing the shelf end, middle part, and offshore end of the cross-slope transect on 06 July 2019.

waters and patchiness in the O_2, chlorophyll and turbidity distributions were observed on scales of 1–10 km. Similarly, the 34.5 isohaline showed fine-scale undulations throughout the transect. This fine-scale variability likely results from vertical motion associated with sub-mesoscale processes occurring on the interface between the shelf and slope/ring waters (Zhang and Partida, 2018).

Analysis of the ship's underway surface water flow on the coat-hanger transect showed that the streamer shelf water was productive. In particular, surface mixed layer NCP was elevated in the streamer shelf water compared to the ring and slope water (Fig. 16a). There is a strong correspondence between SST and NCP, with higher NCP in the streamer water. Moreover, NCP decreased over a north–south-oriented 5-km wide warm filament (at 70.6°W) inside the streamer that stemmed from the slope water from the east, indicating the fine-scale nature of the correspondence between NCP and water mass structure. Attune and IFCB data showed that the elevated surface chlorophyll concentration in the streamer resulted from higher abundance of nanoplankton (2–20 μm) and microplankton (>20 μm) than in the surrounding ring and slope waters (Fig. 16c-d). There was no clear enhancement of picoplankton (<2 μm) biomass in the streamer (Fig. 16b).

4. Discussion

4.1. Streamer subsurface structure

Shelf-water streamers are submesoscale filaments of shelf water entrained offshore by impinging warm-core rings. After leaving the shelf, they often wrap around the rings and thus have a qualitatively similar surface appearance (e.g., Garfield and Evans, 1987; Joyce et al., 1992; Bisagni et al., 2019). However, their subsurface structures can differ. For example, the 1982 shelf water streamer measured by Joyce et al. (1992) at a location 100 km offshore of the shelf break was over 100 m thick, whereas the streamer we observed in July 2019 was only 50 m thick at 80 km offshore of the shelf break, and thus was much thinner than the 1982 streamer. The thickness of a shelf-water streamer is a key parameter for understanding its role in cross-shelf material and energy exchange as studies typically estimate the overall streamer transport based on satellite-measured sea surface information and an assumed depth of the streamer (e.g., Bisagni, 1983).

Shelf-water streamer offshore transport could also occur beneath a surface layer of ring water and be indiscernible via remote sensing. This surface-invisible transport of the shelf water in a *subsurface* layer of 10 s m thick often occurs adjacent to a *surface* shelf water streamer, as both result from entrainment by the ring. The subsurface transport results from submesoscale frontal subduction at the interface of the ring and shelf waters when the shelf water density is higher than the ring water. The density difference forms a density front at their interface (Zhang and Partida, 2018). As the ring migrates shoreward, the density front is intensified, which triggers a secondary flow to counterbalance the frontal intensification (Spall, 1995). Frontal subduction of shelf water is a part of the secondary flow on the shelf side of the interface. Zhang and Partida (2018) demonstrated that this type of subsurface shelf water transport below a surface layer of ring water could be similar in magnitude to the shelf water transport in a surface-visible streamer. However, the cross-streamer transect in July 2019 did not show any subduction of shelf water—in fact, the streamer water tended to overtop

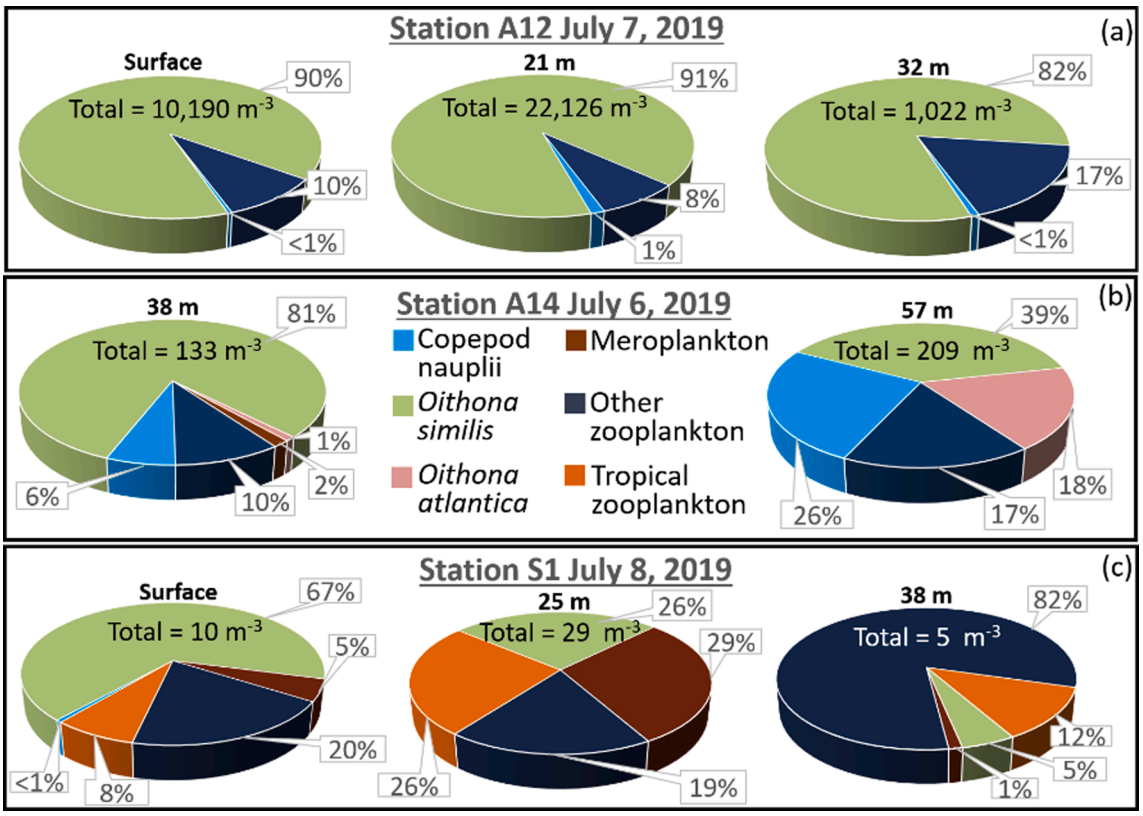

Fig. 11. Metazoan zooplankton community abundance and composition at (a) Station A12 on 07 July, (b) Station A14 on 06 July and (c) Station S1 on 08 July. All zooplankton data were sampled with 150 μm-mesh nets except for Station A14 at 38 m which is from a 100 μm-mesh net.

the ring water when forced by the wind (Fig. 12b), which likely resulted from similarities in the density of the ring and shelf waters (Fig. 12c), a condition different from that described in Zhang and Partida (2018). When a WCR is first formed, its surface density is often lower than the shelf water owing to the much higher temperature (Zhang and Gawarkiewicz, 2015). However, surface ring water can gradually lose its heat and buoyancy through air-sea interactions or mixing with surrounding slope water, and its surface density then increases slowly (Schmitt and Olson, 1985). Alternatively, the increasing downward heat flux from winter to summer could warm the shelf water faster because of the shallower surface mixed layer on the shelf (Zhang et al., 2011), which would tend to reduce the density contrast between shelf and ring waters. SST images indicate that the temperature difference between the surface ring and shelf water decreased from ~ 13 °C in March to ~ 3 °C in July 2019 (Fig. 2). Therefore, before July 2019, the density contrast between ring and shelf waters was likely higher, and there could have been a subsurface layer of shelf water being transported offshore next to the surface streamer. That is, all else being equal, offshore transport of shelf water from March to June was likely substantially higher than that observed in July.

4.2. Impact on slope sea productivity

Both satellite and *in situ* measurements indicate that the streamer carried productive shelf water offshore, as demonstrated by the elevated chlorophyll concentrations (Fig. 3c-j) and surface mixed layer NCP (Fig. 16a) in the streamer shelf water compared to the neighboring surface ring and slope water. Note that *subsurface* chlorophyll in the streamer is not necessarily higher than that in the surrounding slope or ring waters: the measured chlorophyll concentration and productivity at the base of the euphotic zone (50 m) at Station S7 in the slope water to the east of the streamer were higher than those in the streamer (Fig. 14c, h). This elevated subsurface chlorophyll in the slope water resulted from upwelling of the nutrient-rich deep Gulf Stream water (Oliver et al., 2021), and was not detectable in satellite imagery. Therefore, *surface* chlorophyll is not always a good proxy for depth-integrated chlorophyll in the slope sea.

The elevated surface chlorophyll in the streamer relative to the surrounding slope/ring water could result from two different mechanisms: offshore advection of shelf water with high phytoplankton concentrations generated on the shelf before entering the streamer, or sustained local phytoplankton growth in the streamer as the shelf water moves offshore. The former is consistent with high surface *nanoplankton* and *microplankton* biomass in both the streamer and shelf (Fig. 16c-d), but in contrast to the dramatic decrease of surface *picoplankton* biomass from the shelf to the streamer (Fig. 16b). Given the surface-layer flow speed in the streamer of ~ 0.2 m s^{-1}, the time it took the shelf water to travel from A6 to A18 (~90 km apart) was ~ 5 days, which was similar to time scales of phytoplankton mortality and zooplankton grazing in the region (e.g., Fennel et al., 2006). The subsurface chlorophyll concentration at A18 remained elevated with a subsurface maximum similar to that on the inshore end of the transect (Figs. 8e and 10c). This shift in phytoplankton composition and the persistently high NCP in the streamer suggests that at least part of the elevated surface chlorophyll concentration in the streamer was caused by local phytoplankton growth in the streamer, and the high NCP was mostly associated with nanoplankton and microplankton. Additionally, lower zooplankton abundance observed in the streamer shelf water at the offshore station (S1) relative to the inshore stations (A12 and A14) suggests decreased grazing pressure (at least from the > 100 μm size fraction) on the phytoplankton in the streamer, which likely facilitated the local phytoplankton growth.

Phytoplankton growth in the streamer was likely supported by offshore transport of the nutrient-rich subsurface shelf water that was originally below the euphotic zone on the shelf (Fig. 9a-b and 10e-f). Because of the high concentrations of organic material (e.g., CDOM and

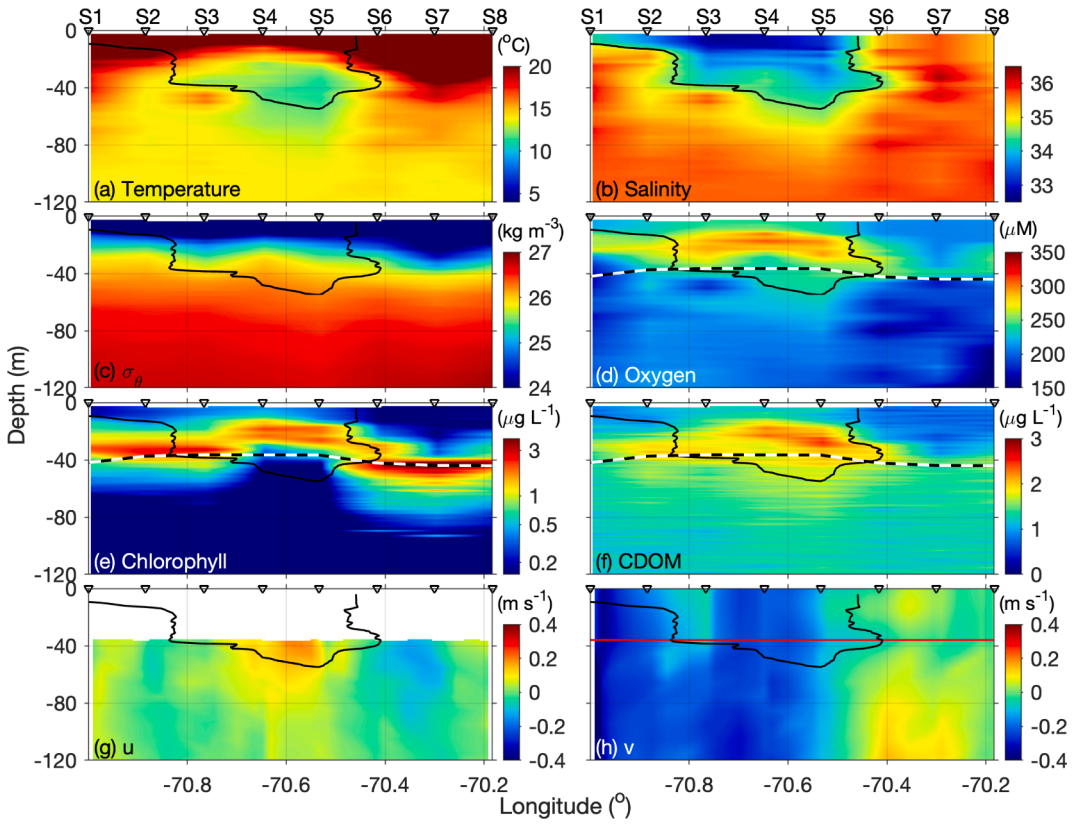

Fig. 12. Cross-streamer distribution of (a) temperature, (b) salinity, (c) σ_θ, (d) oxygen, (e) chlorophyll, (f) colored dissolved organic matter (CDOM), (g) eastward velocity, and (h) northward velocity on 08 July 2019. The black lines are the 34.5 isohaline representing the boundary between the shelf and offshore waters. The triangles on the top of each panel represent locations of the CTD stations. The black-white dashed line represents the base of the euphotic zone; the red line in (k) separates the ADCP-measured v and that computed from thermal-wind balance. (For interpretation of the references to color in this figure legend, the reader is referred to the web version of this article.)

POC; Figs. 8f, 9f), the euphotic zone on the shelf was shallow. The measured 1 % light level at Station A5 on 09 July was at 25 m, and the mean light attenuation coefficient in the surface layer was $k_d = 0.184$ m^{-1}. The nutrients on the shelf below 25 m (Fig. 9a-d) were thus insulated from biological uptake due to light limitation of autotrophs. As the shelf water moved offshore in the streamer, its clarity increased and the light attenuation decreased due to either mixing with surrounding oligotrophic slope and ring waters reducing the CDOM and POC concentrations, or particles gradually sinking from the surface layer. Correspondingly, irradiance penetrated deeper into the water column, and the measured 1 % isolume at Station A18 was at ~ 40 m. The mean light attenuation coefficient in the surface layer at A18 was $k_d = 0.115$ m^{-1}. Given the mean phytoplankton-induced light attenuation coefficient in the region of $k_p = 0.13\ (\mu g\ Chl\ L^{-1})^{-1}\ m^{-1}$ (Oliver et al., 2021), if this decrease of ~ 0.07 m^{-1} in k_d from A5 to A18 resulted entirely from reduction in phytoplankton-induced light attenuation, it would require a decrease in mean chlorophyll concentration of 0.53 $\mu g\ L^{-1}$, which was qualitatively consistent with the observed reduction in surface chlorophyll concentration at the stations (Fig. 10). This change of light attenuation caused an increase in the euphotic zone depths in the offshore portions of the streamer (Fig. 8e-f). Even with a purely horizontal flow (no upwelling), nutrients in the streamer shelf water at 25–40 m would gradually become available for biological consumption as the streamer moved offshore. Consistent with that point, from Station A6 to A18, there was a reduction of NO_3, PO_4 and SiO_4 concentration at that depth range (Fig. 10e-g). Meanwhile, the subsurface chlorophyll maximum deepened from 25 m at Station A6 to 38 m at Station A18 (Fig. 10c). Assuming a vertical diffusivity of 10^{-3} m^2 s^{-1} in the upper 25 m of the streamer, the time for materials at 25 m to be mixed to the surface was ~ 7 days, similar to the streamer water horizontal advection time scale. This suggests that persistence of high NCP in the streamer was supported by deepening of the euphotic zone and utilization of subsurface nutrients. Satellite chlorophyll concentration represents a weighted-average of the chlorophyll signal in the euphotic depth (Morel and Berthon, 1989). The subsurface chlorophyll maximum may have been partially visible at the surface and likely contributed to the elevated chlorophyll concentration in the streamer (relative to ring and slope waters) shown in the satellite images (Fig. 3c-j).

4.3. *Estimated cross-shelf transport*

The measured transport of water, heat, salt and biomass in the shelf water streamer causes exchange between the shelf and deep ocean. Defining shelf water as salinity < 34.5, we estimate the southward streamer volume, heat and salt transport from the cross-streamer CTD transect to be 0.26 Sv, 1.8×10^{13} W and 9.1×10^6 kg s^{-1}, respectively. Applying the same calculation to the southern leg of the VPR coathanger transect yielded transport of 0.18 Sv, 1.2×10^{13} W and 6.3×10^6 kg s^{-1}, respectively. These transport estimates are less than those of the thicker streamer induced by Ring 82B (Table 1; Joyce et al., 1992), but similar to the long-term mean shelf water offshore transport across the shelf break (e.g., Chaudhuri et al., 2009; Ramp et al., 1988).

Mean shelf water chlorophyll concentrations on the cross-streamer section measured by CTD and VPR were 0.80 and 0.60 $\mu g\ L^{-1}$, respectively, while the mean concentrations of POC and DIC were 9.0 $\mu mol\ L^{-1}$ and 2.1 $mmol\ L^{-1}$, respectively. Combining the chlorophyll measurements with the estimated volume transport, and using the Attune and IFCB-based estimate of carbon:chlorophyll mass ratio of 166, we estimate the offshore flux of algal carbon in the streamer to be 3000 mton d

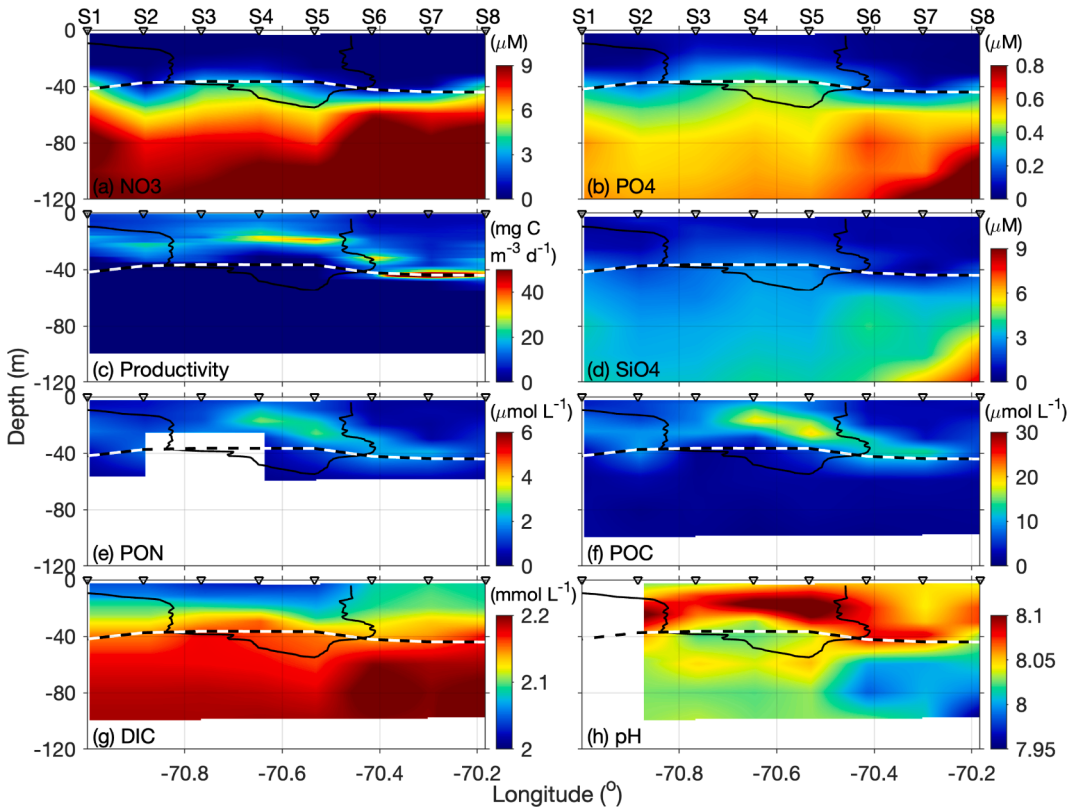

Fig. 13. Cross-streamer distribution of (a) nitrate (NO_3), (b) phosphate (PO_4), (c) modeled primary productivity, (d) silicate (SiO_4), (e) particulate organic nitrogen (PON), (f) particulate organic carbon (POC), (g) dissolved inorganic carbon (DIC), and (h) pH on 08 July 2019. The black lines are the 34.5 isohaline representing the boundary between the shelf and offshore waters. The triangles on the top of each panel represent CTD station locations. The black-white dashed line represents the base of the euphotic zone.

^{1} (2900 mol s^{-1}) and 1500 mton d^{-1} (1600 mol s^{-1}) in the CTD and the VPR transects, respectively. The estimated offshore fluxes of POC and DIC in the shelf- water streamer on the cross-streamer CTD transect were 2400 mton d^{-1} (2340 mol s^{-1}) and 5.7 × 10^5 mton d^{-1} (5.5 × 10^5 mol s^{-1}), respectively. Considering the streamer width of ~ 50 km, all these estimates of instantaneous algal/particulate organic carbon fluxes are greater than the mean cross-shelf carbon export of 1300 mton d^{-1} (1.6 mol s^{-1} km^{-1}) required to balance the horizontal divergence of organic carbon on the entire MAB shelf of ~ 800 km long (Fennel and Wilkin, 2009); the estimated streamer DIC fluxes are two orders of magnitude higher than the model-estimated mean net CO_2 uptake of 2100–3000 mton d^{-1} (1200–2850 mol C s^{-1}) over the entire MAB shelf (~100 × 800 km^2) in 2004–2005 (Fennel and Wilkin, 2009). Mean shelf water O_2 concentrations on the cross-streamer section measured by the CTD and VPR were 257 and 265 mmol m^{-3}, respectively. The corresponding offshore fluxes of O_2 in the streamer were 1.8 × 10^5 mton d^{-1} (6.7 × 10^4 mol s^{-1}) and 1.3 × 10^5 mton d^{-1} (4.8 × 10^4 mol s^{-1}).

Estimating the *net* transport across the shelf break associated with the streamer requires information on characteristics of the volume of water that balances the offshore transport, which was unavailable in July 2019. We here provide two end-member estimates of the net transport (Table 1), and the true transport likely is between the two end-members. On one end (designated as EM1), the offshore volume transport of the shelf water in the streamer from the MAB shelf to the slope sea was completely compensated for by the augmented inflow from upstream (Georges Bank and the Gulf of Maine) to the MAB shelf. The volume of the MAB shelf is conserved. Because properties of the upstream shelf water are presumably similar to those on the MAB shelf (e.g., Lentz, 2010; Wang et al., 2013), in this EM1 case, the aforementioned estimates of volume, heat, salt, carbon and O_2 fluxes in the streamer are *net* shelf-to-slope transport induced by the streamer, and represent an upper bound of the net transport. On the other end (designated as EM2), the offshore volume transport of the shelf water in the streamer could be entirely balanced by onshore intrusion of surface ring water with no net volume transport across the shelf break. This is similar to the assumption of Joyce et al. (1992) to estimate the net cross-shelf transport and also consistent with the observed direct onshore intrusion of WCR water in April 2014 (Zhang and Gawarkiewicz, 2015). However, satellite observations in July 2019 did not show any direct onshore intrusion of the ring water on the surface (Figs. 2, 3). Nevertheless, we provide estimates of the net cross-shelf fluxes in EM2 for reference, as they represent a lower limit of net transport. These estimates utilize the VPR coat-hanger transect to the west of the streamer (west of 71°W; Fig. 15) to define the properties of surface ring water. In EM2, net heat fluxes across the shelf edge estimated from CTD and VPR transects are both shoreward at 1.3 × 10^{12} W; the corresponding net salt fluxes, 5.1 × 10^5 kg s^{-1} and 3.6 × 10^5 kg s^{-1}, are also shoreward. These net heat- and salt flux estimates are an order of magnitude and 50 %, respectively, smaller than those of a shelf-water streamer induced by Ring 82B (Table 1); the differences result from both a weaker volume transport and smaller shelf-ring temperature and salinity differences in July 2019. Nevertheless, this EM2 net shoreward heat flux induced by the streamer in July 2019 is equivalent to a uniform downward heat flux over the entire MAB shelf of ~ 16 W m^{-2}, and the EM2 net salt flux is equivalent to a MAB-wide uniform evaporation rate of 1.1–1.5 cm day^{-1}. Both of these fluxes are significant compared to the annual mean surface heat and freshwater fluxes over the MAB shelf of 10–30 W m^{-2}, and O(1) cm $year^{-1}$ (Lentz, 2010).

Because the surface ring water has a mean chlorophyll concentration of 0.39 μg L^{-1} (top 100 m west of 71°W as measured by the VPR), the EM2 net flux of algal carbon across the shelf edge estimated from the VPR data is 540 mton d^{-1} (520 mol s^{-1}) offshore. If the ring water intruding onto the shelf originates from a depth greater than the upper

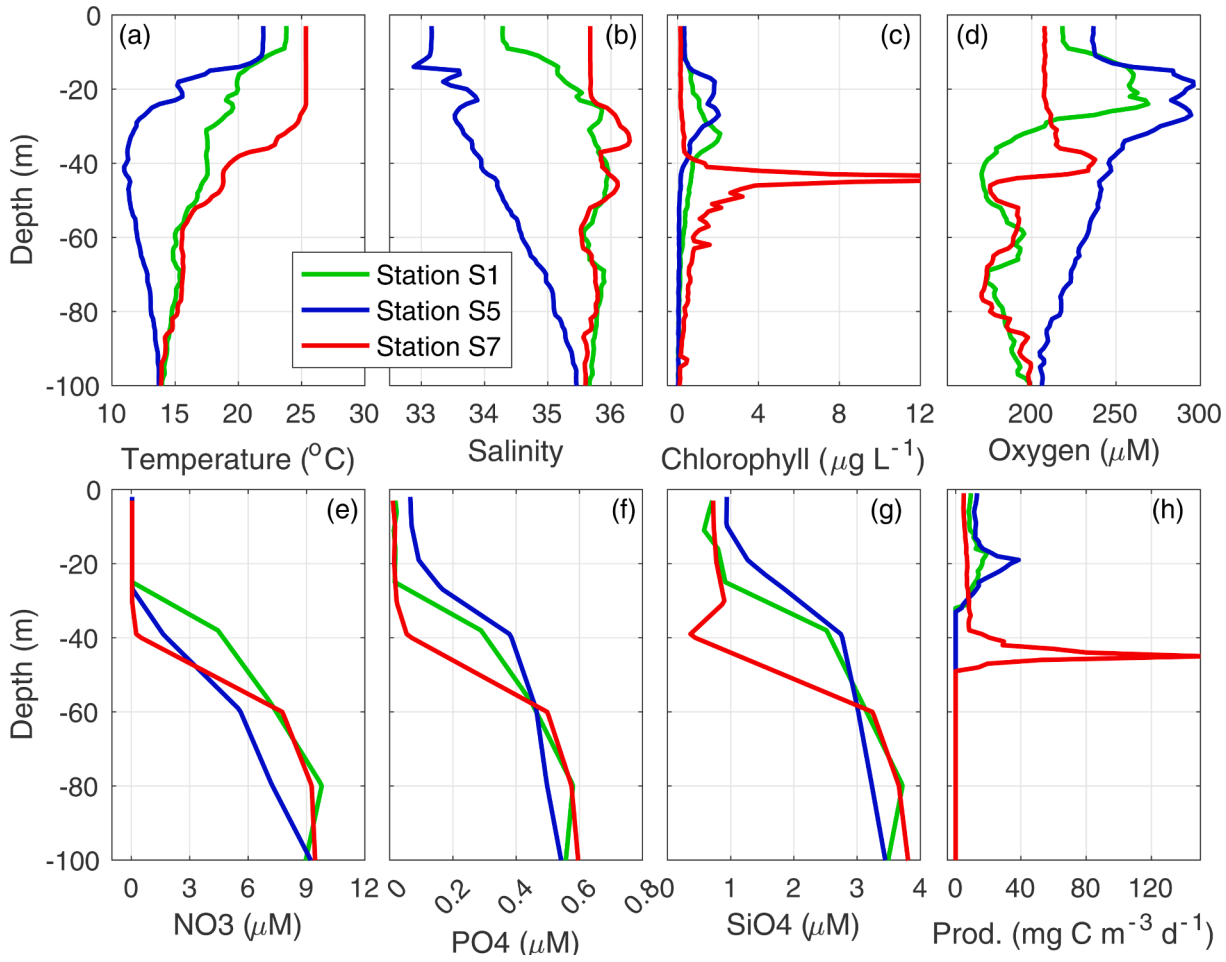

Fig. 14. Vertical profiles of (a) temperature, (b) salinity, and (c) chlorophyll, (d) dissolved oxygen, (e) nitrate, (f) phosphate and (g) silicate concentrations, and (h) modeled primary productivity at Stations S1, S5 and S7, representing the streamer-ring, streamer, and slope waters on the along-slope transect on 08 July 2019. The streamer-ring water at Station S1 is a thin layer of streamer shelf water overlying on top of the ring water.

100 m, the net offshore flux of algal carbon would increase as the deeper ring water had lower chlorophyll concentrations (Fig. 15e). Because the westernmost station (S1; Fig. 4d) on the cross-streamer CTD transect was at 71°W and did not extend into the ring interior, we used the fluorescence and POC data at S1 below the surface layer of streamer water to represent the chlorophyll and POC concentrations of the presumed ring water that intruded onshore. This gives mean chlorophyll and POC concentrations of 0.47 $\mu g\,L^{-1}$ and 3.7 $\mu mol\,L^{-1}$, respectively, which are likely overestimates, as surface chlorophyll concentration tends to decrease westward toward the ring interior (Fig. 15e). Nevertheless, we estimate the net algal carbon and POC exports from the shelf to the deep ocean from the CTD data as 1230 mton d^{-1} (1180 mol s^{-1}) and 1460 mton d^{-1} (1400 mol s^{-1}), respectively. Satellite images (Fig. 2) showed that the ring-shelf contact region spanned about 200 km in the along-shelf direction. Considering the net offshore flux of algal carbon occurring over this ring-shelf contact region, the associated mean cross-shelf algal carbon export rate is 6.2–7.3 mton d^{-1} km^{-1} (5.9–7.0 mol s^{-1} km^{-1}), which is ~ 4 times of the annual mean organic carbon flux required to balance the horizontal divergence of organic carbon on the MAB shelf of 1.6 mton d^{-1} km^{-1} or 1.6 mol s^{-1} km^{-1} (Fennel and Wilkin, 2009). Therefore, streamer-induced shelf-to-deep-ocean export of algal organic carbon during a relatively short-term ring impingement could account for a major proportion of the long-term mean offshore export of organic carbon at the shelf break.

To estimate the EM2 net flux of *inorganic* carbon across the shelf edge, we used the subsurface (13–100 m) data at the western DIC station (Station S2) to represent the DIC concentration of the presumed ring water that intruded onshore. This gives a mean ring water DIC concentration of 2.16 $mmol\,L^{-1}$ and a net inorganic carbon *import* from the deep ocean to the shelf of 1.6×10^4 mton d^{-1} (1.5×10^4 mol C s^{-1}), an estimate larger than the model-estimated air-to-sea net CO_2 flux over the entire MAB shelf in 2004–2005 (Fennel and Wilkin, 2009). The net fluxes of O_2 estimated from the CTD and VPR data were 3.7×10^4 mton d^{-1} (1.3×10^4 mol s^{-1}) and 1.8×10^4 mton d^{-1} (6.3×10^3 mol s^{-1}), both offshore. These heat, salt, carbon and O_2 EM2 net transport estimates are smaller than the fluxes induced by the streamer associated with Ring 82B estimated by Joyce et al. (1992) (Table 1).

These end-member estimates provide a range of the streamer-associated cross-shelf net fluxes during the July 2019 cruise, which is an instantaneous assessment of streamer fluxes that took place over the 5-month period of ring-shelf interaction. Lack of subsurface measurements makes it impossible to directly calculate fluxes of the shelf water streamer at other times within these 5 months. As a result, it is unclear how representative the CTD/VPR-based estimates of fluxes are. However, as stated in Section 4.1, the ring-induced offshore volume flux of shelf water before July 2019 was likely higher than the estimates provided here, implying that POC and O_2 fluxes in the streamer were greater during spring. If biogeochemical properties of the shelf and ring waters remained unchanged over the entire period, higher volume flux in the streamer would suggest higher net offshore transport of POC and O_2. Satellite data actually show surface chlorophyll concentrations in the streamer of 1–3 $\mu g\,L^{-1}$ in March-June, higher than that (~0.5 $\mu g\,L^{-1}$) in early July (Fig. 3). The surface chlorophyll concentrations in the ring did not change substantially from March to July. If these surface

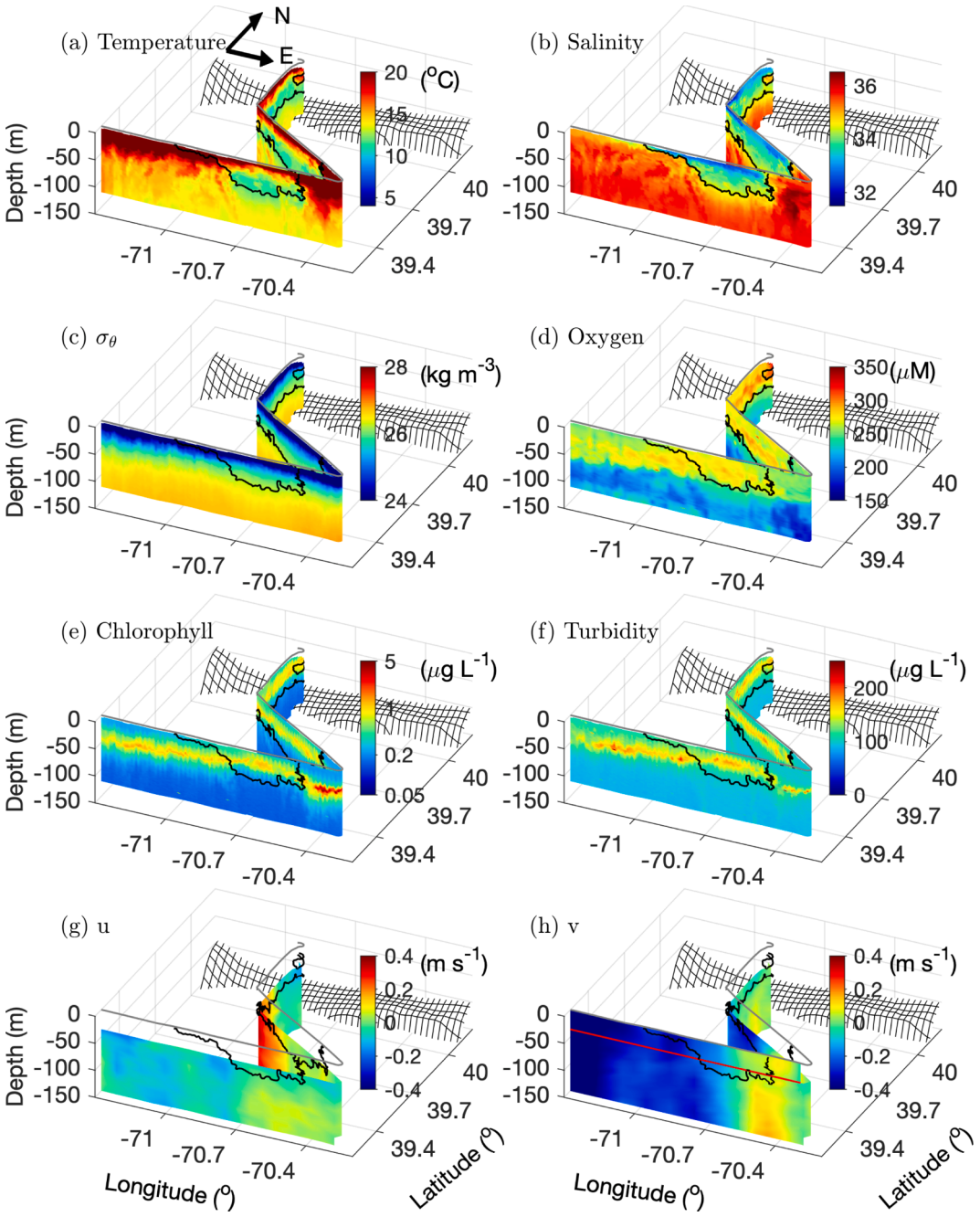

Fig. 15. VPR-measured distributions of (a) temperature, (b) salinity, (c) σ_θ, (d) oxygen, (e) chlorophyll, (f) turbidity, (g) u, and (h) v. The black lines represent the 34.5 isohaline, the boundary between the shelf and offshore waters. The red line in (h) separates the ADCP-measured v below and that computed from thermal-wind balance. The grey line depicts the track of the VPR tow on the surface. The black grids represent the seafloor. The arrows in (a) depict the north and east directions. (For interpretation of the references to color in this figure legend, the reader is referred to the web version of this article.)

concentration data represent the entire streamer layer and the surface ring water, both the offshore POC flux in the streamer and the associated net offshore POC transport would be higher. Assuming the streamer-volume POC and O_2 fluxes decreased linearly from March through August, the estimates in early July would be lower than the mean fluxes over the entire period. That is, the mean cross-shelf net fluxes of water, heat, salt, POC and O_2 induced by Ring 19C in March-August 2019 were likely greater than the instantaneous fluxes estimated for early July.

5. Summary

Shelf-water streamers are distinctive submesoscale features in the deep Mid-Atlantic Bight (MAB) slope sea that are visible from space. They are formed by warm-core rings (WCR) impinging on the shelf edge entraining shelf water moving offshore. Shelf-water streamers are an important mechanism of water exchange between the continental shelf and the neighboring deep slope sea. Few studies have examined their subsurface pattern and provided a robust quantification of the associated cross-shelf fluxes. This study focuses on a WCR in 2019 and the shelf-water streamer it generated over the period of March-August. The evolution of the ring and streamer is examined by analyzing satellite-measured sea surface height, temperature, and chlorophyll. *In situ* measurements from a two-week cruise in July 2019 were used to examine the vertical distributions of physical, biological and

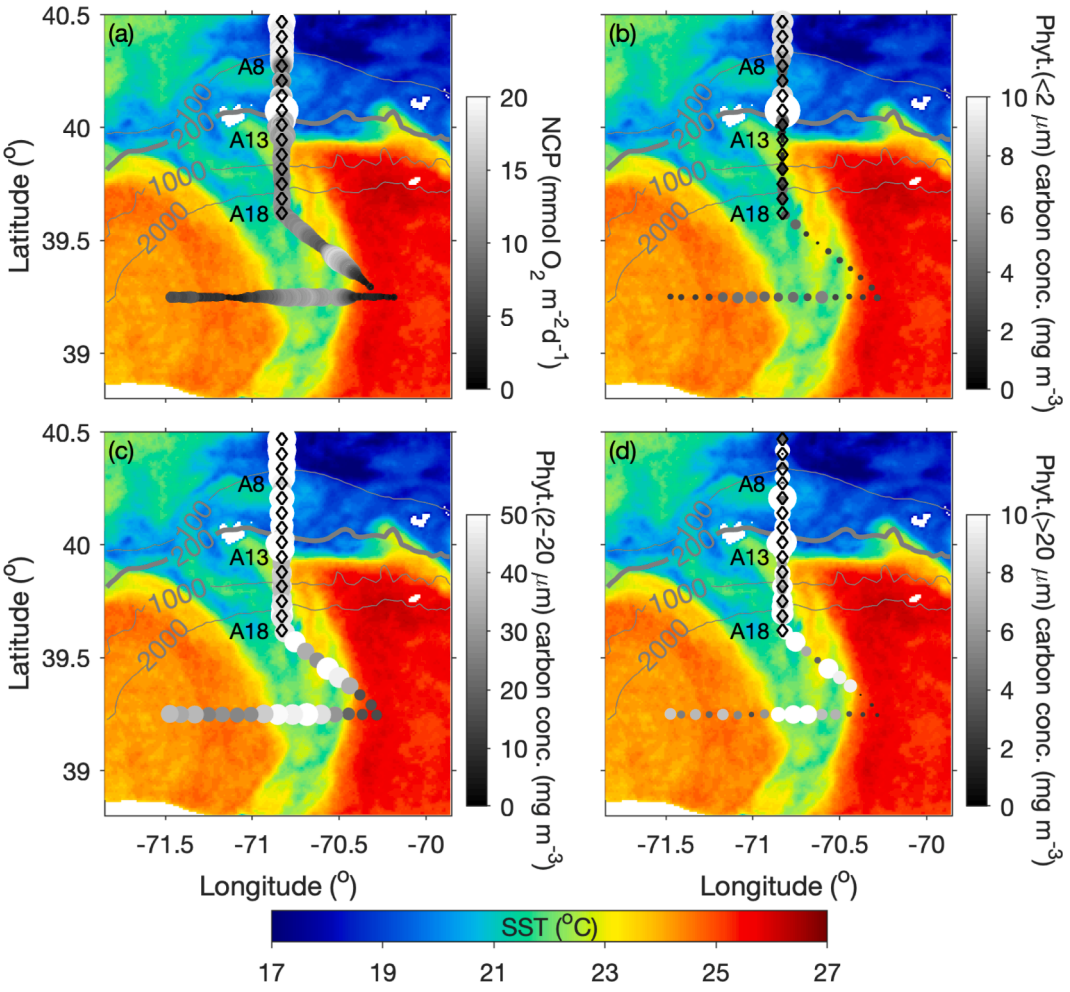

Fig. 16. Spatial distribution of sea surface temperature on 8 July 2019 (color) and (a) net community production (NCP) and carbon concentrations of phytoplankton of (b) $< 2\mu$ m, (c) 2-20μ m and (d) $> 20\mu$ m in the surface layer as determined from the underway measurements on 7–8 July 2019 (gray circles). The size and grey color of the circles depict the magnitude of the NCP and phytoplankton carbon concentrations, and the circles' size is not to scale across the panels. The diamonds depict locations of the cross-shelf CTD stations. Gray lines are isobath contours.

biogeochemical properties in the streamer and to estimate the associated cross-shelf fluxes of water, heat, salt, carbon, and O_2.

Our estimates of the streamer-associated fluxes represent a snapshot of the 5-month long exchange process at the shelf edge. These estimates demonstrate that the streamer-induced substantial offshore transport of shelf water, heat, salt, carbon and O_2. When we assume the offshore streamer transport is volumetrically balanced by increased inflow from the upstream shelf, the associated offshore fluxes of heat, salt, organic and inorganic carbon, and O_2 in the streamer represent the net cross-shelf fluxes. These are all significant compared to other related fluxes estimated at the shelf break. In another scenario, we assume that the offshore streamer transport is volumetrically balanced by onshore transport of surface ring water. The associated net cross-shelf fluxes of heat, salt and inorganic carbon are shoreward, and the net fluxes of organic carbon and O_2 are offshore. The estimated heat, salt, O_2 and organic carbon fluxes in the second scenario are smaller than those estimated from a streamer formed by a WCR in 1982 (Joyce et al., 1992). Nonetheless, the estimated net heat and salt fluxes in July 2019 are significant compared to the air-sea exchange on the shelf and also to the indirectly estimated heat and salt eddy fluxes across the edge of the entire MAB shelf (Lentz, 2010). The streamer-associated net flux of algal/particulate organic carbon is similar to a model-estimated total organic carbon export from the entire MAB to the open ocean (Fennel and Wilkin 2009); the net flux of inorganic carbon is much larger than the model-estimated mean CO_2 update over the entire MAB shelf. Therefore, shelf-water streamers represent a major form of exchange between the MAB shelf and open ocean. These fluxes depend critically on the vertical structure of the streamers, including not only their thickness but also the degree of subduction that takes place at the interface between the streamer and the ring (Zhang and Partida, 2018).

The surface biological productivity was higher in the shelf-water streamer than in the surrounding ring and slope waters. This enhancement of the surface productivity likely resulted from nutrient-rich subsurface shelf water being carried offshore in the streamer. Due to the overlying shelf water mixing with the oligotrophic slope and ring waters, or the particles in the shelf water sinking out of the surface layer, the euphotic zone in the streamer deepened. This allowed subsurface nutrients to be consumed, resulting in enhanced productivity and biomass of larger (nano-to-micro) phytoplankton size classes in the surface streamer water. Decreased zooplankton abundance in the streamer presumably facilitated local growth of the phytoplankton.

The recent increase in the number of WCRs forming in the slope sea off the northeast coast of the North America (Gangopadhyay et al., 2019) will likely lead to more ring-shelf interaction and more shelf-water streamers. As a result, streamer-associated shelf-ocean exchange of heat, salt and materials and their influence on physical, biological and biogeochemical processes in the shelf and slope seas presumably have increased as well. To better understand how this region will respond to climate change from both physical and biological perspectives, the dynamics of these streamers and the fluxes they bring about must be better

Table 1
EM1 (Streamer offshore flux) and EM2 (net flux when streamer transport is balanced by ring water onshore intrusion) fluxes of water, heat, salt, organic carbon, inorganic carbon, and dissolved oxygen estimated from the *in situ* measurement in July 2019 and their comparison with relevant fluxes in other studies.

Flux variable	Unit	Method	EM1	EM2	EM1 estimates in Joyce et al (1992)	EM2 estimates in Joyce et al (1992)	Other comparisons
Volume flux	Sv (10^6 m^3 s^{-1})	CTD	−0.26	0	−0.38	–	−0.28* (a streamer in 2016); −0.13§ (annual mean entrainment of shelf water by WCRs)
		VPR	−0.18	0			
Heat flux	10^{12} W	CTD	−18	1.3	–	18	160–320‡ (Mean cross-shelf eddy heat flux over the entire MAB shelf break)
		VPR	−12	1.3			
Salt flux	10^5 kg s^{-1}	CTD	−91	5.1	–	9.4	5.6‡ (Mean cross-shelf eddy salt flux over the entire MAB shelf break)
		VPR	−63	3.6			
Algal organic carbon flux	10^4 mton day^{-1}	CTD	−0.3	−0.12	–	–	−0.13† (Total organic carbon flux across the entire MAB shelf break)
		VPR	−0.15	−0.054			
Particulate organic carbon flux	10^4 mton day^{-1}	POC	−0.24	−0.15	−1.6 (Suspended Particulate Matter)	−0.41 (Suspended Particulate Matter)	
Inorganic carbon flux	10^4 mton day^{-1}	DIC	−57	1.6	–	–	0.21–0.3† (mean net CO_2 uptake over the entire MAB shelf)
Oxygen flux	10^4 mol s^{-1}	CTD	−6.7	−1.3	−23	−2.8	–
		VPR	−4.8	−0.63			

* Chen et al (2014).
§ Chaudhuri et al. (2009).
‡ Lentz (2010).
† Fennel and Wilkin (2009).

quantified.

Declaration of Competing Interest

The authors declare that they have no known competing financial interests or personal relationships that could have appeared to influence the work reported in this paper.

Data availability

MWIR SST are produced by Remote Sensing Systems and sponsored by NASA, and the data are publicly available at www.remss.com. The MODIS Aqua SST were produced by NASA Goddard Space Flight Center, Ocean Ecology Laboratory, Ocean Biology Processing Group, and the data are publicly available at https://oceancolor.gsfc.nasa.gov/. The AVHRR SST data were obtained from the MARACOOS THREDDS server (http://tds.maracoos.org/thredds/catalog.html). The MODIS Aqua SSC data were obtained from the publicly available ERDDAP server (https://basin.ceoe.udel.edu/erddap/griddap/index.html) maintained by the Ocean Exploration, Remote Sensing and Biogeography Laboratory led by Dr. Matthew Oliver at University of Delaware. The gridded SSH data were downloaded from the European Union Copernicus Marine Environmental Monitoring Service (https://marine.copernicus.eu/) with product user manual at http://marine.copernicus.eu/documents/PUM/CMEMS-SL-PUM-008-032-062.pdf. The SSH-based eddy detection package, OceanEddies, is publicly available at https://github.com/ifrenger/OceanEddies. SPIROPA CTD and VPR data are archived at the Biological and Chemical Oceanography Data Management Office (BCO-DMO) project page: https://www.bco-dmo.org/project/748894. The ship-mounted ADCP data are available on the R2R Data Repository (https://www.rvdata.us/search/cruise/TN368).

Acknowledgements

This research was supported by the National Science Foundation (OCE-1657803, OCE-1657855, OCE-1657489, OCE-1658054, and OCE-1655686) and the Dalio Explorer Fund. We thank Canbo Xiao and Yilang Xu for the CTD operations; Josh Eaton and Fredrik Thwaites for the VPR operations; Frannie Adams, Erin Kim, and Lumi Kinjo for contributing to O_2/Ar data collection; Mar Arroyo, Olivia De Meo and Elizabeth Shadwick for the DIC data collection and analyses; Margaret Mulholland, Dreux Chappell, Sophie Clayton, Corday Selden and Yifan Zhu for discussions during the course of the study, and other SPIROPA colleagues and crew of the *R/V Thomas G. Thompson* for their support at sea. We also thank Olga Kosnyrev for the post-cruise data processing.

References

Andres, M., 2016. On the recent destabilization of the Gulf Stream Path downstream of Cape Hatteras. Geophys. Res. Lett. 43, 9836–9842. https://doi.org/10.1002/2016GL069966.
Bisagni, J.J., 1983. Lagrangian current measurements within the eastern margin of a warm-core Gulf Stream ring. J. Phys. Oceanogr. 13, 709–715. https://doi.org/10.1175/1520-0485(1983)013<0709:LCMWTE>2.0.CO;2.
Bisagni, J.J., Nicolas, O.C., Pettipas, R., 2019. Interannual variability of Gulf Stream warm-core ring interactions with the outer continental shelf and potential broad scale relationships with longfin squid (*Doryteuthis pealeii*) relative abundance, 1981–2004. ICES J. Mar. Sci. 76, 1257–1270. https://doi.org/10.1093/icesjms/fsz144.
Biscaye, P.E., Flagg, C.N., Falkowski, P.G., 1994. The shelf edge exchange processes experiment, SEEP-II: An introduction to hypotheses, results and conclusions. Deep-Sea Res. II 41, 231–252. https://doi.org/10.1016/0967-0645(94)90022-1.
Cassar, N., Barnett, B.A., Bender, M.L., Kaiser, J., Hamme, R.C., Tilbrook, B., 2009. Continuous high-frequency dissolved O_2/Ar measurements by equilibrator inlet mass spectrometry. Anal. Chem. 81 (5), 1855–1864.
Chapman, D.C., Beardsley, R.C., 1989. On the origin of shelf water in the Middle Atlantic Bight. J. Phys. Oceanogr. 19 (3), 384–391.
Chen, K., He, R., Powell, B.S., Gawarkiewicz, G.G., Moore, A.M., Arango, H.G., 2014. Data assimilative modeling investigation of Gulf Stream Warm Core Ring interaction with continental shelf and slope circulation. J. Geophys. Res. 119, 5968–5991. https://doi.org/10.1002/2014JC009898.
Cherian, D.A., Brink, K.H., 2016. Offshore transport of shelf water by deep-ocean eddies. J. Phys. Oceanogr. 46, 3599–3621. https://doi.org/10.1175/JPO-D-16-0085.1.
Csanady, G.T., Hamilton, P., 1988. Circulation of slopewater. Cont. Shelf Res. 8, 565–624. https://doi.org/10.1016/0278-4343(88)90068-4.
Davis, C.S., Thwaites, F.T., Gallager, S.M., Hu, Q., 2005. A three-axis fast-tow digital Video Plankton Recorder for rapid surveys of plankton taxa and hydrography. Limnol. Oceanogr.: Meth. 3, 59–74. https://doi.org/10.4319/lom.2005.3.59.
Dickson, A.G., Sabine, C.L., Christian, J.R. (Eds.), 2007. Guide to Best Practices for Ocean CO_2 measurement. PICES Special Publication, Sidney, British Columbia, p. 3.
Egbert, G.D., Erofeeva, S.Y., 2002. Efficient inverse modeling of barotropic ocean tides. J. Atmosph. Ocean. Tech. 19, 183–204. https://doi.org/10.1175/1520-0426(2002)019<0183:EIMOBO>2.0.CO;2.
Evans, R.H., Baker, K.S., Brown, O.B., Smith, R.C., 1985. Chronology of warm-core ring 82B. J. Geophys. Res. 90, 8803–8811.

Faghmous, J.H., Frenger, I., Yao, Y., Warmka, R., Lindell, A., Kumar, V., 2015. A daily global mesoscale ocean eddy dataset from satellite altimetry. Scien. Data 2, 150028. https://doi.org/10.1038/sdata.2015.28.

Falkowski, P.G., Flagg, C.N., Rowe, G.T., Smith, S.L., Whitledge, T.E., Wirick, C.D., 1988. The fate of a spring phytoplankton bloom: export or oxidation? Cont. Shelf Res. 8 (5-7), 457–484.

Fennel, K., Wilkin, J., 2009. Quantifying biological carbon export for the northwest North Atlantic continental shelves. Geophys. Res. Letters 36, L18605. https://doi.org/10.1029/2009GL039818.

Flierl, G.R., Wroblewski, J.S., 1985. The possible influence of warm core Gulf Stream rings upon shelf water larval fish distribution. Fish. Bull. 83, 313–330.

Gangopadhyay, A., Gawarkiewicz, G., Silva, E.N., Monim, M., Clark, J., 2019. An observed regime shift in the formation of warm core rings from the Gulf Stream. Scien. Rep. 9, 12319. https://doi.org/10.1038/s41598-019-48661-9.

Gangopadhyay, A., Gawarkiewicz, G., Nishchitha, E., Silva, S., Silver, A.M., Monim, M., Clark, J., 2020. A census of the warm-core rings of the Gulf Stream: 1980–2017. e2019JC016033 J. Geophys. Res. 125. https://doi.org/10.1029/2019JC016033.

Gardner, W.D., Richardson, M.J., Smith, W.O., 2000. Seasonal patterns of water column particulate organic carbon and fluxes in the Ross Sea, Antarctica. Deep-Sea Res. II 47 (15-16), 3423–3449.

Garfield, N., Evans, D.L., 1987. Shelf water entrainment by Gulf Stream warm-core rings. J. Geophys. Res. 92 (C12), 13003.

Hales, B., Vaillancourt, R.D., Prieto, L., Marra, J., Houghton, R., Hebert, D., 2009. High-resolution surveys of the biogeochemistry of the New England shelfbreak front during Summer, 2002. J. Mar. Syst. 78, 426–441. https://doi.org/10.1016/j.jmarsys.2008.11.024.

JGOFS, 1996. Protocols for the Joint Global Ocean Flux Study (JGOFS) core measurements. IOC SCOR Report 19. Bergen, Norway.

Joyce, T.M., Bishop, J.K.B., Brown, O.B., 1992. Observations of offshore shelf water transport induced by a warm-core ring. Deep-Sea Res. 39, S97–S113.

Lee, C.M., Brink, K.H., 2010. Observations of storm-induced mixing and Gulf Stream Ring incursion over the southern flank of Georges Bank: Winter and summer 1997. J. Geophys. Res. 115, C08008. https://doi.org/10.1029/2009JC005706.

Lentz, S.J., 2010. The mean along-isobath heat and salt balances over the Middle Atlantic Bight continental shelf. J. Phys. Oceanogr. 40, 934–948. https://doi.org/10.1175/2009JPO4214.1.

Linder, C.A., Gawarkiewicz, G., 1998. A climatology of the shelfbreak front in the Middle Atlantic Bight. J. Geophys. Res. 103 (C9), 18405–18423.

Ma, J., Smith Jr., W.O., 2022. Primary productivity in the Mid-Atlantic Bight: Is the shelf break a location of enhanced productivity? Frontiers Mar. Sci. 9, 824303 https://doi.org/10.3389/fmars.2022.824303.

Moberg, E.A., Sosik, H.M., 2012. Distance map to estimate cell volume from two-dimensional plankton images. Limnology and Oceanography, Methods 10, 278–288. https://doi.org/10.4319/lom.2012.10.278.

Morel, A., Berthon, J.-F., 1989. Surface pigments, algal biomass profiles, and potential production of the euphotic layer: Relationships reinvestigated in view of remote-sensing applications. Limnol. Oceanogr. 34, 1545–1562. https://doi.org/10.4319/lo.1989.34.8.1545.

Morgan, C.W., Bishop, J.M., 1977. An example of Gulf Stream eddy-induced water exchange in the Mid-Atlantic Bight. J. Phys. Oceanogr. 7 (3), 472–479.

Myers, R.A., Drinkwater, K., 1989. The influence of Gulf Stream warm core rings on recruitment of fish in the northwest Atlantic. J. Mar. Res. 47, 635–656. https://doi.org/10.1357/002224089785076208.

Oliver, H., Zhang, W.G., Smith, W.O., Alatalo, P., Chappell, P.D., Hirzel, A.J., Selden, C. R., Sosik, H.M., Stanley, R.H.R., Zhu, Y., McGillicuddy, D.J., 2021. Diatom hotspots driven by western boundary current instability. Geophys. Res. Let. 48 (11) https://doi.org/10.1029/2020GL091943.

Petitpas, C.M., Turner, J.T., Deeds, J.R., Keafer, B.A., McGillicuddy Jr, D.J., Milligan, P. J., Shue, V., White, K.D., Anderson, D.M., 2014. PSP toxin levels and plankton community composition and abundance in size-fractionated vertical profiles during spring/summer blooms of the toxic dinoflagellate *Alexandrium fundyense* in the Gulf of Maine and on Georges Bank, 2007, 2008, and 2010. 2 Plankton community composition and abundance. Deep-Sea Res. II 103, 350–367. https://doi.org/10.1016/j.dsr2.2013.04.012.

Ramp, S.R., Brown, W.S., Beardsley, R.C., 1988. The Nantucket Shoals Flux Experiment 3. The alongshelf transport of volume, heat, salt, and nitrogen. J. Geophys. Res. 93, 14039–14054. https://doi.org/10.1029/JC093iC11p14039.

Ricciardulli, L., Wentz, F.J., 2004. Uncertainties in sea surface temperature retrievals from space: Comparison of microwave and infrared observations from TRMM. J. Geophys. Res. 109, C12013. https://doi.org/10.1029/2003JC002247.

Rypina, I.I., Llopiz, J.K., Pratt, L.J., Lozier, M.S., 2014. Dispersal pathways of American eel larvae from the Sargasso Sea. Limnol. Oceanogr. 59, 1704–1714. https://doi.org/10.4319/lo.2014.59.5.1704.

Saunders, P.M., 1971. Anticyclonic eddies formed from shoreward meanders of the Gulf Stream. Deep-Sea Res. 18, 1207–1219. https://doi.org/10.1016/0011-7471(71)90027-1.

Schmitt, R.W., Olson, D.B., 1985. Wintertime convection in Warm-Core Rings: thermocline ventilation and the formation of mesoscale lenses. J. Geophys. Res. 90, 8823–8837. https://doi.org/10.1029/JC090iC05p08823.

Seguro, I., Marca, A.D., Painting, S.J., Shutler, J.D., Suggett, D.J., Kaiser, J., 2019. High-resolution net and gross biological production during a Celtic Sea spring bloom. Prog. Oceanogr. 177, 101885. https://doi.org/10.1016/j.pocean.2017.12.003.

Sherman, K., Kane, J., Murawski, S., Overholtz, W., Solow, A., 2002. The U.S. northeast shelf large marine ecosystem: Zooplankton trends in fish biomass recovery. In: Sherman, K., Skjoldal, H.R. (Eds.), Large Marine Ecosystems of the North Atlantic: Changing States and Sustainability. Elsevier Science B.V, Amsterdam, The Netherlands, pp. 195–215.

Smith Jr., W.O., Marra, J., Hiscock, M.R., Barber, R.T., 2000. The seasonal cycle of phytoplankton biomass and primary productivity in the Ross Sea. Antarctica. Deep-Sea Res. II 47, 3119–3140.

Smith, W.O., Zhang, W.G., Hirzel, A., Stanley, R.M., Meyer, M.G., Sosik, H., Alatalo, P., Oliver, H., Sandwith, Z., Crockford, E.T., Peacock, E.E., Mehta, A., McGillicuddy, D. J., 2021. A regional, early spring bloom of *Phaeocystis pouchetii* on the New England continental shelf. J. Geophys. Res. 126 (2) https://doi.org/10.1029/2020JC016856.

Sosik, H.M., Futrelle, J., Brownlee, E.F., Peacock, E., Crockford, T., Olson, R.J., 2016: hsosik/ifcb-analysis: IFCB-Analysis software system, initial formal release at v2 feature stage (Version v2.0) . Zenodo. doi: 10.5281/zenodo.153978.

Sosik, H.M., Olson, R.J., 2007. Automated taxonomic classification of phytoplankton sampled with imaging-in-flow cytometry. Limnol. Oceanogr.: Meth. 5 (6), 204–216.

Sosik, H.M., R. J. Olson, E. V. Armbrust. 2010. Flow cytometry in phytoplankton research. In: D.J. Suggett, O. Prasil, M.A. Borowitzka (Eds.), Chlorophyll a fluorescence in aquatic sciences: Methods and Applications, *Developments in Applied Phycology*, vol. 4, Springer, 171–185, doi: 10.1007/978-90-481-9268-7_8.

Spall, M.A., 1995. Frontogenesis, subduction, and cross-front exchange at upper ocean fronts. J. Geophys. Res. 100, 2543–2557. https://doi.org/10.1029/94JC02860.

Stanley, R.M., Sandwith, Z., Williams, W.J., 2015. Rates of summertime biological productivity in the Beaufort Gyre: a comparison between the low and record-low ice conditions of August 2011 and 2012. J. Mar. Sys. 147, 29–44.

Ullman, D.S., Codiga, D.L., Pfeiffer-Herbert, A., Kincaid, C.R., 2014. An anomalous near-bottom cross-shelf intrusion of slope water on the southern New England continental shelf. J. Geophys. Res. 119 (3), 1739–1753.

Vaillancourt, R.D., Marra, J., Prieto, L., Houghton, R.W., Hales, B., Hebert, D., 2005. Light absorption and scattering by particles and CDOM at the New England shelfbreak front. Geochem., Geophys., Geosyst. 6 (11).

van Heuven, S., Pierrot, D., Rae, J.W.B., Lewis, E., Wallace, D.W.R., 2011. MATLAB program developed for CO_2 system calculations. ORNL/CDIAC-105b. Carbon Dioxide Information Analysis Center, Oak Ridge National Laboratory, U.S. Department of Energy. doi: 10.3334/CDIAC/otg.CO2SYS_MATLAB_v1.1.

Walsh, J.J., Biscaye, P.E., Csanady, G.T., 1988. The 1983–1984 shelf edge exchange processes (SEEP)—I experiment: hypotheses and highlights. Cont. Shelf Res. 8, 435–456. https://doi.org/10.1016/0278-4343(88)90063-5.

Wang, Z.A., Wanninkhof, R., Cai, W.-J., Byrne, R.H., Hu, X., Peng, T.-H., Huang, W.-J., 2013. The marine inorganic carbon system along the Gulf of Mexico and Atlantic coasts of the United States: Insights from a transregional coastal carbon study. Limnol. Oceanogr. 58, 325–342. https://doi.org/10.4319/lo.2013.58.1.0325.

Wiebe, P.H., Burt, K.H., Boyd, S.H., Morton, A.W., 1976. A multiple opening/closing net and environmental sensing system for sampling zooplankton. J. Mar. Res. 34, 313–326.

Zhang, W.G., Gawarkiewicz, G.G., McGillicuddy, D.J., Wilkin, J.L., 2011. Climatological mean circulation at the New England shelf break. J. Phys. Oceanogr. 41, 1874–1893. https://doi.org/10.1175/2011JPO4604.1.

Zhang, W.G., Gawarkiewicz, G.G., 2015. Dynamics of the direct intrusion of gulf stream ring water onto the mid-Atlantic bight shelf. Geophys. Res. Lett. 42, 7687–7695. https://doi.org/10.1002/2015GL065530.

Zhang, W.G., Partida, J., 2018. Frontal subduction of the Mid-Atlantic Bight shelf water at the onshore edge of a warm-core ring. J. Geophys. Res. 123, 7795–7818. https://doi.org/10.1029/2018JC013794.